NASA CR-132503

MEASUREMENT AND CORRELATION OF AERODYNAMIC HEATING TO SURFACE CORRUGATION STIFFENED STRUCTURES IN THICK TURBULENT BOUNDARY LAYERS

by

H.J. Brandon and R.V. Masek

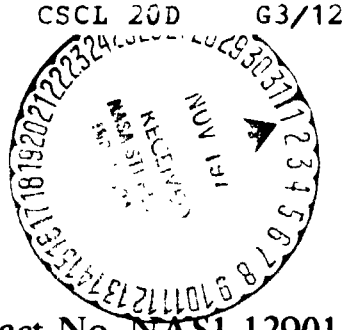

Prepared Under Contract No. NAS1-12901

by

MCDONNELL DOUGLAS ASTRONAUTICS COMPANY-EAST

St. Louis, Missouri 63166 (314) 232-0232

for

NATIONAL AERONAUTICS AND SPACE ADMINISTRATION

NASA CR-132503

MEASUREMENT AND CORRELATION OF AERODYNAMIC HEATING TO SURFACE CORRUGATION STIFFENED STRUCTURES IN THICK TURBULENT BOUNDARY LAYERS

by

H.J. Brandon and R.V. Masek

Prepared Under Contract No. NAS1-12901

by

MCDONNELL DOUGLAS ASTRONAUTICS COMPANY-EAST

St. Louis, Missouri 63166 (314) 232-0232

for

NATIONAL AERONAUTICS AND SPACE ADMINISTRATION

FOREWORD

This report summarizes the work conducted by McDonnell Douglas Astronautics Company-East (MDAC-E) in St. Louis, Missouri for the NASA Langley Research Center under Contract NAS1-12901. Mr. James C. Dunavant was the NASA Technical Monitor for this study. L. A. Haas (MDAC-E) made a significant contribution to those parts of this study which involved the lateral heat conduction investigation and application of the developed flow model. Using his method, R. B. Dirling (MDAC-W) calculated the average heat transfer values which are presented herein.

TABLE OF CONTENTS

1.0 SUMMARY

The results of an experimental program to evaluate heat transfer and pressure distributions on corrugation roughened flat plates in thick turbulent boundary layers have been correlated and compared with similar data and correlations for thin boundary layers. The experimental program consisted of tests in the tunnel wall boundary layers of the Langley Unitary Plan Wind Tunnel (UPWT) and Continuous Flow Hypersonic Tunnel (CFHT) at free-stream Mach numbers of 2.5, 3.5, 4.5, and 10.3. Tests in the UPWT were conducted at a free-stream Reynolds number/cm of 0.108×10^6 and in the CFHT, at a Reynolds number/cm of 0.033×10^6 and 0.013×10^6. The test configurations consisted of 50.8 cm x 50.8 cm panels with corrugated beads of two different peak amplitudes, 0.61 cm and 0.29 cm. The angle of the corrugated beads relative to the flow direction was varied between 0° (aligned) and 90° (normal). The peak and average heating were found to be strong functions of the Mach number and Reynolds number. The better correlations of the thick boundary layer data incorporated an internal parameter in the undisturbed boundary layer (total temperature at the height corresponding to the roughness amplitude) and boundary layer bulk parameters (δ^* and θ) in addition to the boundary layer edge and geometric parameters. In general, poor agreement of the present results with the correlations and data of previous investigators was noted. This is not unexpected since the roughness elements tested in this study were deeply submerged in the boundary layer, whereas the previous investigators had a more limited data base obtained in thin turbulent boundary layers.

2.0 INTRODUCTION

The effect of surface corrugations and surface irregularities on boundary layers has received much attention in the last ten years (References 1 to 5). Most of the results obtained in these investigations are summarized by Bertram in Reference 6. Bertram's work, although quite extensive, did not include data for which the boundary layer was orders of magnitude thicker than the surface corrugation height. This is an important practical problem because very thick turbulent boundary layers are often encountered under certain flight conditions. The present study is concerned with heat transfer when the corrugations are deeply submerged in a thick turbulent boundary layer.

The flow conditions for which heating distributions have been measured on corrugated surfaces and wavy walls in turbulent boundary layers are shown in Figure 1, which gives the ratio of the displacement thickness to the roughness height versus the local edge Mach number for an equivalent smooth surface. The present data are seen to greatly extend the range of data available on corrugated surfaces in turbulent boundary layers. These data were obtained by testing fullscale corrugation roughened panels in the wall boundary layer of a supersonic and hypersonic wind tunnel.

In this report, the experimental program used to obtain the data is described. The data are analyzed and correlated in terms of the pertinent flow and geometric parameters. The developed correlations are compared with the available thin boundary layer data, and the present data are also compared with previously published correlation techniques.

3.0 MODEL AND INSTRUMENTATION

Two corrugation roughened flat panels were tested in this study. Both plates were 50.8 cm x 50.8 cm x 2.54 cm and were fabricated from nominally 0.043 cm thick 321 stainless steel. A photograph of one of the panels is shown in Figure 2, and a drawing of the panel shape is presented in Figure 3. The two panels were identical in shape except for the wave amplitude, as shown in Figure 3. The peak amplitude was 0.61 cm for one panel and 0.29 cm for the other panel. For both panels the maximum amplitude was a maximum and essentially constant over an 18.8 cm section in the center, and tapered to zero at 1.91 cm from the panel edge. Each plate contained 12 1/2 corrugations (wave cycles) which ran the entire length of the model. With the corrugations aligned parallel with the flow (configuration termed $\emptyset$ - 0°), the corrugations were composed of parabolic segments. With the corrugations aligned normal to the flow (termed $\emptyset$ = 90°), the corrugations were constructed of circular arcs connected by straight line segments. For both plates, the wavelength was equal to 3.66 cm.

Wave shapes (or corrugation shapes) for the two panels as a function of the flow angle relative to the corrugations are shown in Figures 4 and 5, and the surface distances along the waves in the direction of the flow are presented in Figures 6 and 7. The wave shape is greatly influenced by the flow angle. The local surface angle along the wave, α, is shown in Figure 8 for both panels for $\emptyset$ = 90°. For the larger corrugation, the maximum angle is + 60°, and for the smaller corrugation, the maximum surface angle is + 22°. As the angle $\emptyset$ decreases, the angle α also decreases so that $\pm$ 60° and $\pm$ 22° represent the maximum and minimum surface angles for all values of $\emptyset$.

Both corrugated models were instrumented with thermocouples and pressure orifices. With the waves normal to the flow direction, the 2nd, 6th, and 10th waves were instrumented with thermocouples along the model centerline in the direction of the flow (Figures 9 and 10). In the same fashion, the pressure taps were located on the 2nd and 10th waves slightly off the centerline (Figures 11 and 12).

A smooth flat plate (50.8 cm x 50.8 cm x 2.54 cm) was also fabricated from 321 stainless steel (0.127 cm thick). This model was instrumented with thermocouples only. Flat plate heating data were measured so that the heating data obtained on the corrugation roughened panels could be referenced to local measured flat plate values.

4.0 TEST PROGRAM

The two corrugated panels and the flat plate were tested in the turbulent wall boundary layer of the Langley Unitary Plan Wind Tunnel (UPWT) and the Continuous Flow Hypersonic Tunnel (CFHT). The panels were attached to an adapter plate which was mounted flush with the wind tunnel wall as shown schematically in Figure 13. For the UPWT tests, the adapter plate contained a mechanical actuator assembly so that the corrugation orientation angle relative to the free-stream direction could be varied from 0° to 90°. For the CFHT tests, the corrugations could only be tested from 0° to 15° and from 75° to 90° due to the arrangement of the injection mechanism.

The flow and geometric conditions for the present study are listed in Table I. The flat plate was also tested at the five different Mach number and Reynolds number combinations. The boundary layer parameters for the turbulent wall boundary layers are listed in Table II. The displacement thickness and momentum thickness for the CFHT were calculated from measured pitot and total temperature profiles through the boundary layer by assuming a constant free-stream static pressure through the boundary layer. At the time of these calculations, no static pressure measurements through the boundary layer were available. For the UPWT, δ^* and θ were obtained by calculating the boundary layer development on the wind tunnel wall using the numerical method described by Keller and Cebeci (Reference 7). This method has been extended to compressible flows by Cebeci, and this latter computer program was used for the present calculations. Good agreement was obtained in a comparison of the velocity profiles predicted by this method and the experimental velocity profiles measured by Couch (Reference 8). Beckwith's correlation (Reference 9) was used to calculate the laminar sublayer thickness for the CFHT. This correlation, however, did not contain data in the range of interest for the UPWT test conditions. Therefore, for the UPWT conditions, δ_s was calculated from the following equation (Reference 10):

$$\delta_s = \frac{11\mu_w a_w}{\gamma P_{FP} M_\infty \sqrt{\frac{C_f}{2}}} \qquad (1)$$

where C_f was taken from the boundary layer solution. δ_s values calculated in this manner are superimposed on Beckwith's correlation (Figure 14). Fairly good agreement exists between these calculations and an extrapolation of the Beckwith correlation.

5.0 EXPERIMENTAL RESULTS

In this section the heating and pressure distributions on corrugation roughened surfaces deeply submerged in thick turbulent boundary layers are presented. External flow and geometric conditions were varied so that the effect of Mach number, Reynolds number, flow angle, and roughness height could be determined.

Flat Plate Distributions - The measured spanwise heating distributions on the flat plate, shown in Figures 15 and 16 , revealed gradients in the wall boundary layers of both the UPWT and CFHT in the vertical direction. These gradients are due to the manner in which the boundary layer develops in the nozzle. The gradients in the UPWT wall boundary layer are less severe than in the CFHT. This is probably due to the fact that the constant area test section of the UPWT is located approximately 7 feet downstream of the end of the nozzle. This constant area section allows the gradients in the boundary layer to dampen out. The axial gradient in the flat plate heating distributions was negligible for both the UPWT and the CFHT.

Elimination of Spanwise Gradient Effects - Data taken on the corrugated panels exhibited similar spanwise heating gradients to those observed on the flat plate. However, analysis of the corrugated heating data showed that the effects of the nonuniform boundary layer could be eliminated by referencing the corrugated heating data to the local flat plate value, as shown in Figure 17. In this figure, nondimensionalized heating distributions on a wave at three spanwise locations (y=0, 16.51, and -16.51 cm) are shown for the case in which the corrugations were normal to the flow. Normalizing the corrugated panel heat transfer coefficients by the local flat plate value collapses the three different spanwise distributions. For this reason all the distributions on the corrugation roughened surfaces reported in this study are nondimensionalized and correlated with the local flat plate value.

Flow Angle (Corrugation Angle) Effect - Heat transfer and pressure distributions for supersonic flow (M_∞ = 3.5, Re_∞/cm = .108 x 10^6) are presented in Figure 18 for flow angles of 0^o, 15^o, and 90^o and are presented for hypersonic flow (M_∞ = 10.3, Re_∞/cm = .033 x 10^6) in Figure 19 for flow angles of 0^o, 15^o, 75^o, and 90^o. Results are for the larger amplitude panel. Both heat transfer and pressure are ratioed to measured flat plate values. The largest heating and pressure increases occur when the flow is normal to the corrugations. For all flow angles heating is much more affected than pressure. The largest changes in heating occur between $\emptyset$=0 and 15^o. These trends are similar to those observed for thin boundary layers (Reference 6). Oil flows indicated that these distributions were caused by flow separation in the valley and subsequent reattachment on the following wave. The surface pressure is essentially equal to the flat plate pressure except in the region of flow reattachment. The same effect of flow angle was measured on the smaller amplitude panel.

Mach Number Effect - During the supersonic tests in the UPWT, the Mach number was varied while the Reynolds number was held constant at $Re_\infty/cm = .108 \times 10^6$. As can be seen in Figure 20, the Mach number has a big effect on the heating distribution and only a slight effect on the pressure distribution. These results are for the flow normal to the corrugations having a peak amplitude of 0.61 cm. The free-stream Mach number had the same effect on the panel which had a peak amplitude of 0.29 cm.

Reynolds Number Effect - As with the Mach number, the Reynolds number strongly influences the heating distribution and only slightly changes the pressure distribution (Figure 21). This case is for the free-stream flow direction normal to the deep corrugation. These trends were measured in CFHT in which the Mach number was held constant at $M_\infty = 10.3$ and the Reynolds number was changed from $Re_\infty/cm = .013 \times 10^6$ to $.033 \times 10^6$. Again, similar results were obtained with the shallow wave panel in that peak heating and pressure increased with Reynolds number in the same magnitude relative to the respective flat plate value. It should be noted that this trend differs from the thin boundary layer data. The thin boundary layer data of Cary (Reference 4) indicate that the peak heating is inversely proportional to the Reynolds number, whereas the current data indicate a direct proportionality.

Wave Amplitude Effect - The present tests on the effect of corrugation height (amplitude) in thick turbulent boundary layers yielded results which are radically different than those for thin boundary layers. In the present study, heat transfer and pressure were found to be relatively insensitive to the wave amplitude for all flow conditions investigated. This observation, demonstrated in Figures 22 and 23, indicates that the effect of wave height is much less than the effect of Mach number and Reynolds number. This result can prove to be very important in the sizing of corrugated heat shield panels designed for vehicle application in very thick boundary layers. For example, using the data of Cary for thin boundary layers which were obtained for approximately the same free-stream conditions and geometric parameters as for the present supersonic test, the effect of increasing the wave height by a factor of two would be to increase the peak heating by a factor of nearly three. This result shows that caution must be exercised in extrapolating thin boundary layer data to predict the heating for currugation roughened surfaces designed for use in very thick boundary layers.

Wave Cycle Effect - In previous results, peak heating and pressure on multiple waves in thin turbulent boundary layers were found to decrease with increasing wave cycle. These decreases were not found for the present data in thick turbulent boundary layers. In fact no decay in peak heating or pressure was detected for the present tests for a succession of corrugations. This result is clearly seen in Figures 24 and 25 which present heating distributions over the 2nd, 6th, and 10th waves and pressure distributions over the 2nd and 10th waves. It is clear from these figures that for a given set of flow conditions, the heating and pressure distributions for the entire panel are independent of wave cycle. This result suggests that surface

roughness deeply submerged in the boundary layer has a small effect on the external flow. In fact, the external flow adjusts so rapidly to the disturbance of the wave that each succeeding wave experiences the same incoming temperature and velocity profile as the preceding wave. This was verified from pitot profiles taken through the boundary layer at the end of the corrugated panels which were almost identical to the smooth wall pro[illegible] On the other hand, wave cycles located in thin boundary layers drastically effect the external flow conditions (References 4 and 6) which results in significant decreases in heating and pressure.

6.0 CORRELATION OF PRESENT TEST RESULTS

The maximum and average wave heating measured during this study are summarized in Tables III and IV. Maximum values were obtained from careful fairings of the data. The average heating is based on the projected (flat plate) area and not the true surface area. These average values were obtained by integrating the area under the heating distributions and applying a surface area correction. For almost all flow conditions, significant increases in peak heating occur for all flow angles greater than 0^{o}. For hypersonic conditions, the average heating is less than the flat plate value for several flow angles. However, for the supersonic tests, all average heating values were observed to be greater than the flat plate value except when the corrugations were aligned in the free stream flow direction.

Theoretical Flow Model - Oil flow patterns were obtained during both the supersonic and hypersonic tests. These photos did not reveal detailed surface flow patterns, but indicated flow separation just aft of the wave peak and reattachment on the following wave for even small wave angles (the smallest wave angle for which oil flows were taken was 15^{o}). A flow model (Figure 26) consistent with the oil flow patterns was postulated in hope that the heating distribution on complete wave could be predicted. In this model, flow separation is assumed to occur near the top of the wave and an upstream and downstream attached boundary layer are assumed to initiate at the reattachment point (which is approximated by the location of the measured peak pressure). Edge stagnation conditions for the two new boundary layers are assumed to be those at the reattachment point. These stagnation conditions are used in conjunction with the measured surface pressures to define local edge conditions which are used as input to a nonsimilar compressible turbulent boundary layer solution for a flat plate (see Test Program for discussion of the solution). The stagnation pressure at the reattachment point is obtained by the following technique. First, the static pressure on the streamline at reattachment is assumed equal to the free-stream flat plate pressure. Second, the total pressure on this streamline is estimated. The surface pressure at the reattachment point is then calculated and compared with the measured surface pressure. This procedure is repeated until the calculated pressure equals the measured pressure. The total temperature at the reattachment point is assumed to correspond to the total temperature in the undisturbed (flat plate) boundary layer at the vertical location for which the local stagnation pressure equals the stagnation pressure at the reattachment point.

Prediction of the heating distribution using the flow model is shown in Figure 27 for a supersonic case ($M_{\infty} = 4.5$, $Re_{\infty}/cm = 0.108 \times 10^{6}$) with the flow normal to the waves. The theory follows the trend of the data, but the predicted values are higher than the measured values. It was found that the predicted heating distribution was primarily a function of the total temperature at the reattachment point. Certainly more analysis is needed to improve and assess the range of validity of the flow model.

Correlation of Peak Heating - One of the main objectives of this investigation was to correlate the peak heating data in terms of the flow conditions and geometric parameters. Preliminary sensitivity studies showed that the peak heating for the flow normal to the waves could be correlated in terms of the local Mach number in the flat plate boundary layer evaluated at the maximum wave amplitude (Figure 28). Also, experience with the flow model indicated that a dominant factor in the theory which controlled the magnitude of the heating prediction was the total temperature at the reattachment point. These two findings suggested that an internal boundary layer temperature parameter evaluated at the peak amplitude would be useful in correlating the data. The parameter decided upon is

$$\bar{\theta} = \frac{T_{T_e} - T_w}{T_{T_\infty} - T_w} \tag{2}$$

A similar parameter was employed to change the heat transfer coefficient predicted using the theoretical flow model from one based on the temperature at reattachment to one based on the free-stream temperature (with the exception that $T_{T_{RP}}$ was used instead of the T_{T_e} in the actual conversion).

The first attempt at correlating the data in terms of the temperature parameter $\bar{\theta}$ proved quite successful, as shown in Figure 20. With the term

$$h_{max}/h_{FP}\,\frac{1}{\bar{\theta}}$$

as the dependent variable, the present data for the flow normal to the waves are directly proportional to the Mach number, shape factor, and the square root of the wave amplitude/wave length and inversely proportional to the Reynolds number based on the wave amplitude. Some of the Cary data, shown in Figure 29, also agree with this correlation. (The $\bar{\theta}$ used for Cary's data was 1). However, comparison of this correlating form with the present data for other flow angles showed that different forms of the governing parameters would be needed.

An automated multiple regression technique designed to fit multiple variables was employed to help sort out the important parameters and obtain consistent nonbiased correlating equations. The computer program, which is described in detail in Reference 11, is a stepwise Multiple Regression Analysis (MRA) which provides information as to the adequacy of candidate correlation functions and the equation coefficients. The MRA computes a series of multiple linear regression equations in a stepwise manner. At each step, one parameter is added to the equation. The variable that is added is the one which makes the greatest reduction in the variance about the mean.

Several good fits to all the present data were obtained with $h_{max}/h_{FP}\,\frac{1}{\bar{\theta}}$ as the dependent variable. However, these data fits were found to be in poor agreement with the other data sets. Further analysis showed that if

$$\left(h_{max}/h_{FP}\,\frac{1}{\bar{\theta}} - 1\right)$$

was used as the dependent variable, all the present data could be modelled and much better agreement existed between the correlations and the other data sets. The following equations were found to give good fits to the present data:

$$\frac{h_{MAX}}{h_{FP}}\,\frac{1}{\bar{\theta}} - 1 = \frac{C_1}{M_\infty^{.615}}\left(\frac{\varepsilon}{L}\right)^{.334} \frac{1}{R_{e\varepsilon}^{.607}}\left(\frac{\delta^*}{L}\right)^{.898} \frac{1}{\left(\frac{\theta}{L}\right)^{1.043}} \qquad (3)$$

$$\frac{h_{MAX}}{h_{FP}} - 1 = \frac{C_2}{M_\infty^{.98}}\left(\frac{\varepsilon}{L}\right)^{.147} \frac{1}{R_{e\varepsilon}^{.203}}\left(\frac{\delta^*}{L}\right)^{1.57} \frac{\bar{\theta}^{.882}}{\left(\frac{\theta}{L}\right)^{1.393}} \qquad (4)$$

where $C_1 = e^{7.512}$

$C_2 = e^{2.19}$

Note that $\bar{\theta}$ was an independent variable in the derivation of Equation (4).

Equation (3) is compared with the present data for all flow angles in Figure 30. A good fit to the data was also obtained by Equation (4).

During the course of the correlation activity, it was discovered that another important geometric parameter was the sine of the local surface angle at reattachment. It could intuitively be expected that a parameter representing a normal component to the surface at reattachment would play a role in correlating the data. It was found that by including sine α as a variable,

the temperature parameter $\bar{\theta}$ could be eliminated from the list of variables. Two correlations developed using the sine are:

$$\left(\frac{h_{MAX}}{h_{FP}} - 1 \right) \frac{1}{\sin \alpha} = C_3 M_\infty^{1.097} \frac{1}{\left(\frac{\varepsilon}{L}\right)^{.526}} R_{e\varepsilon}^{.42} \left(\frac{\delta^*}{L}\right)^{.148} \frac{1}{\left(\frac{\theta}{L}\right)^{.208}} \quad (5)$$

$$\frac{h_{MAX}}{h_{FP}} - 1 = \frac{C_4}{M_\infty^{1.457}} \frac{1}{\left(\frac{\varepsilon}{L}\right)^{.206}} R_{e\varepsilon}^{.514} \left(\frac{\delta^*}{L}\right)^{2.104} \frac{1}{\left(\frac{\theta}{L}\right)^{1.387}} \frac{1}{(\sin \alpha)^{.196}} \quad (6)$$

where $C_3 = \frac{1}{e^{6.614}}$

$C_4 = \frac{1}{e^{6.486}}$

Again, Equation (6) was derived assuming sin α was an independent variable.

The sine of the surface angle at reattachment is listed in Table V along with the sine of the maximum surface angle which is also listed for comparison. As example of the data fit obtained, Equation (5) is compared with the 33 data points in Figure 31. Equally good agreement between correlation and data points was also obtained by Equation (6).

Equations (4) to (6) show vastly different sensitivities to the individual parameters. Yet each equation represents a good fit of the data. This result is due to a lack of data obtained in experiments for which the parameters were varied independently.

7.0 COMPARISON WITH OTHER DATA SOURCES AND CORRELATIONS

The thin turbulent boundary layer data available on surface corrugations and surface irregularities are listed in Table VI and are compared with the present data set in this section. Comparison of these other data sets with Equations (3) through (6) showed that only one of the correlations gave a prediction which was in the ball park for all these data sets. The disagreement of the thin boundary layer data with the present results is demonstrated in Figure 32, which is a comparison with Equation (3). The Shore data (Reference 1) and the Stallings data point (Reference 2) agree fairly well with the correlation. However, all the other data sets fall well below the correlation. The best agreement with the other data sets was obtained with Equation (5) and this equation is compared with all the data in Figure 33. Although there is considerable scatter, the data do tend to group around this correlation.

Bertram (Reference 4) found that Jaeck's correlation (Reference 3) gave a fair to good estimate of the maximum heating trends for thin turbulent boundary layers. Jaeck's correlation is compared with the present data obtained in thick turbulent boundary layers for various Mach numbers (Figure 34) and Reynolds numbers (Figure 35) as a function of the flow angle, $\emptyset$. Jaeck's correlation greatly underpredicts the data for thick boundary layers for all flow conditions and all flow angles. Also shown in these figures are distributions predicted by Equation (3) which closely represent the data. Based on these results, it appears Jaeck's correlation is not valid for corrugation roughened surfaces deeply submerged in thick boundary layers where flow separation occurs. As discussed by Cary (Reference 4), Jaeck's theory gave a good estimate for thin boundary layers except when the boundary layer was separated prior to the wave. Where there was extensive separation, the theory seriously underestimated the maximum heating, as in the present case.

Average heat transfer to rough surfaces for reentry conditions has received much attention in the past few years. As a result, several correlations of rough surface average heat transfer have been proposed. A simple approximate turbulent heating formulation developed by Powars (Reference 12) was believed to be one of the more reliable approaches.

Average heat transfer values from the present experiments are compared with the Powars correlation in Figure 36. The equivalent sand grain roughness, k_e, used in this correlation was calculated using Dirling's analysis (Reference 13). It is seen that the data fall well below the Powars equation for $10k_e/\delta_s > 10$. This surprising disagreement led to a further analysis of the average heating data using the recent method proposed by Dirling. It was found that for the flow normal to the shallow waves, the average heating could be predicted within a few percent using Dirling's method. However, it was also found that the deep wave data could only be predicted if the equivalent sand grain roughness height was based on the wave half-height. Using this half-height, the average heating could also be predicted within a few

percent. The reason for this phenomenon is not completely understood and needs more investigation. A summary comparison of the present average heating data and the Dirling theory is shown in Table VII.

The variation in the heating rate with the local pressure is shown in Figure 37. This correlation reveals two separate relationships. In the separated region ($P \leq P_{FP}$), the heating is independent of pressure. In the attached flow regime, the heating ratio is approximately proportional to the square of the pressure ratio rather than the eight tenths power, which more nearly represents the reattachment heating for thin turbulent boundary layers. Therefore, for roughness deeply submerged in a turbulent boundary layer, the increase over flat plate heating is much greater than the corresponding increase over flat plate pressure.

8.0 CONCLUSION

An extensive set of tests has been conducted on corrugation roughened surfaces in the thick turbulent wall boundary layers of the Langley Unitary Plan Wind Tunnel (UPWT) and the Continuous Flow Hypersonic Tunnel (CFHT). Tests in the UPWT were conducted at free-stream Mach numbers of 2.5, 3.5, and 4.5, and a free-stream Reynolds number/cm of 0.108×10^6. Tests in the CFHT were conducted at a free-stream Mach number of 10.3, and free-stream Reynolds numbers/cm of 0.033×10^6 and 0.013×10^6. Analysis of the data obtained in this study yielded the following conclusions:

1. Large increases in heating were measured for all corrugation angles greater than 0°. As with thin boundary layers, the largest changes occurred for small sweep angles.

2. Significant effects of Mach number and Reynolds number were detected. The present peak heating data indicated a direct proportionality to Reynolds number, whereas the thin boundary layer data were inversely proportional to Reynolds number.

3. In contrast to the data for thin boundary layers, the heating distributions for the flow normal to the waves were found to be essentially independent of wave amplitude/wave length and wave cycle.

4. The local heating was found to be proportional to the square of the pressure, rather than the eight tenths power which approximates the thin boundary layer reattachment relation. For the present data changes in pressure were much less than the corresponding changes in heating due to the corrugations.

5. A flow model was postulated to predict the entire wave heating distribution. For a supersonic case ($M_\infty = 4.5$), the flow model followed the trend of the data, but the predicted values were higher than the measured values.

6. Based on a total temperature in the undisturbed boundary layer at the wave height, the maximum heat transfer coefficient data for the flow normal to the waves correlated with

$$\frac{M_\infty}{Re_\varepsilon} \quad \frac{\delta^*}{\theta} \quad \left(\frac{\varepsilon}{L}\right)^{.5}$$

7. For all flow orientation angles, the peak heating data were correlated in terms of bulk boundary layer, internal boundary layer, and geometric parameters. Data for thin boundary layers were found to group around one of the correlations developed from the present thick boundary layer data.

8. Jaeck's correlation greatly underpredicted the maximum heating data for all flow conditions and all flow angles.

9. Average heating values were found to fall well below the Powars correlation.

10. Dirling's method was found to predict the average heating within a few percent for the smaller amplitude wave. Also, by using an equivalent sand grain roughness based on the wave half-height, this method also matched the average heating values for the larger amplitude wave.

9.0 REFERENCES

1. Shore, C. P., Dixon, S. C., and Griffith, G. E., "Experimental Pressures and Turbulent Heat Transfer Coefficients Associated With Sinusoidal Protuberances on a Flat Plate at a Mach Number of 3," NASA TN D-1626, March 1963.

2. Stallings, R. L., Jr. and Collins, I. K., "Heat Transfer Measurements on a Flat Plate and Attached Protuberances in a Turbulent Boundary Layer at Mach Numbers of 2.65, 3.51, and 4.44," NASA TN D-2428, September 1964.

3. Jaeck, C. L., "Analysis of Pressure and Heat Transfer Tests on Surface Roughness Elements with Laminar and Turbulent Boundary Layers," NASA CR-537, 1966.

4. Cary, A. M., Jr. and Morrisette, E. L., "Effect of Two-Dimensional Multiple Sine-Wave Protrusions on the Pressure and Heat Transfer Distributions for a Flat Plate at Mach 6," NASA TN D-4437, March 1968.

5. Weinstein, L. M., "Effects of Two-Dimensional Sinusoidal Waves on Heat Transfer and Pressure Over a Flat Plate at Mach 8," NASA TN D-5937, Aug 1970.

6. Bertram, M. H., Weinstein, A. M., Cary, A. M., Jr., and Arrington, J. P., "Heat Transfer to a Wavy Wall in Hypersonic Flow," AIAA Journal, Vol. 5, No. 10, October 1967.

7. Keller, H. B. and Cebeci, T., "Accurate Numerical Methods for Boundary Layer Flows," AIAA Paper 71-164, January 1971

8. Couch, L. M., "Flow Field Measurements Downstream of Two Protuberances on a Flat Plate Submerged in a Turbulent Boundary Layer at Mach 2.49 and 4.44," NASA TN D-5297, July 1969.

9. Beckwith, I. E., Harvey, W. D., and Clark, F. L., "Comparison of Turbulent Boundary Layer Measurements at Mach Number 19.5 With Theory and an Assessment of Probe Errors," NASA TN D-6192, June 1971.

10. Reda, D. C., "Compressible Turbulent Skin Friction on Rough and Rough/Wavy Walls in Adiabatic Flow," NOLTR 74-34, February 1974.

11. Christensen, H. E. and Kipp, H. W., "Data Correlation and Analysis of Arc Tunnel and Wind Tunnel Tests of RSI Joints and Gaps," MDC Rpt. E1003, January 1974.

12. Third Quarterly Progress Report for Thermomechanical-Thermochemical Evaluation of Advanced RV Nose Tip Concerts Utilizing the Ballistic Range, Aerotherm Corp., March 1971.

13. Dirling, R. B., Jr., "A Method for Computing Roughwall Heat Transfer Rates on Reentry Nosetips," AIAA Paper No. 73-763, 8th Thermophysics Conference, July 1973.

14. Haas, L. A., "HEATRAN: General Heat Transfer Program," Unpublished Memorandum, MDAC-E, July 1972.

10.0 LIST OF SYMBOLS

a	speed of sound
C_f	skin friction coefficient
CFHT	Continuous Flow Hypersonic Tunnel
h	heat transfer coefficient
k_e	equivalent sand-grain roughness height
L	wavelength in direction of flow
M_∞	free-stream Mach number
P	static pressure
Re_∞	free-stream Reynolds number, $\frac{\rho_\infty U_\infty}{\mu_\infty}$
Re_ε	Reynolds number based on wave amplitude, $\frac{\rho_\infty U_\infty \varepsilon}{\mu_\infty}$
S	surface distance measured from top of wave
T	temperature
UPWT	Unitary Plan Wind Tunnel
U	velocity
X	axial distance measured from top of wave
Y	spanwise distance along tunnel sidewall; also wave vertical coordinate
α	local wave surface angle
γ	ratio of specific heats
ε	maximum wave amplitude (See Figure 3-C)
δ_s	laminar sublayer thickness
δ^*	displacement thickness
δ	boundary layer thickness
θ	momentum thickness

$\overline{\theta}$	temperature parameter (See Equation (2))
μ	molecular viscosity
ϕ	angle of corrugations relative to free-stream flow direction (See Figure 3-A)
ρ	density

SUBSCRIPTS

$( )_T$	stagnation conditions
$( )_w$	wall conditions
$( )_{av}$	average
$( )_{FP}$	flat plate
$( )_{MAX}$	maximum
$( )_\varepsilon$	evaluated at maximum wave amplitude
$( )_\infty$	free-stream conditions
$( )_{RP}$	reattachment point
$( )_{\phi = 90°}$	evaluated for flow normal to corrugation
$( )_{TOTAL}$	total distance

APPENDIX A

CONDUCTION CORRECTIONS FOR THE UPWT DATA

Because of the technique used to obtain the heat transfer coefficients in the UPWT (Reference 2), coupled with the thickness of the panel skin and the small size of the waves, lateral heat conduction corrections were found to be significant. The UPWT data reduction procedure used to evaluate conduction corrections (Reference 2) assumed that the cross-sectional area between thermocouple nodes was constant. However, due to the process used to fabricate the corrugated panels, the cross-sectional area was not uniform for the deep panel. For this reason, the effect of non-uniform area on the lateral heat conduction correction was investigated for the UPWT data.

A comparison of the Langley calculations and the present analysis (Reference 14) for one-dimensional heating (i.e., using the measured temperature-time histories directly without including lateral heating) is shown in Figure A-1 for the heating distribution over the wave for $M_\infty = 4.45$ and the flow normal to the waves. This case was chosen because it was felt that it was the most severe with regard to the importance of heat conduction since it represented the largest heating gradient for the UPWT test. Both sets of calculations give essentially the same wave heat distribution. The effect of lateral heat conduction on these distributions is shown in Figure A-2 which compares the Langley and the present calculations. Again both sets of calculations agree very closely. Also, the variable area effect is quite small. Based on these results, it was concluded that the Langley calculations, which included lateral heat conduction and assumed a constant area between the nodes, gave an accurate representation of the wave heating distribution.

TABLE I TEST CONDITIONS

WAVE HEIGHT, cm	TYPE OF DATA	ϕ, DEG	M_∞	Re_∞/cm	T_w/T_{T_∞}
.61	HEAT TRANSFER AND PRESSURE	0.7.5,15,30,60, 90	2.5,3.5,4.5	$.108X10^6$	.81
.29	HEAT TRANSFER AND PRESSURE	0,30,90	2.5,3.5,4.5	$.108X10^6$	.81
.61 .29	HEAT TRANSFER AND PRESSURE	0,15,75,90	10.3	$.033X10^6$ $0.13X10^6$	.30

NOTE: WAVE LENGTH = 3.66 cm FOR BOTH MODELS.

TABLE II BOUNDARY LAYER PARAMETERS

M_∞	R_{e_∞}/cm	δ^*, cm	θ, cm	δ_s, cm	$\varepsilon = 0.61$cm $\frac{\delta^*}{\theta}$	$\varepsilon = 0.29$cm $\frac{\delta^*}{\theta}$
2.5	0.108×10^6	2.87	0.83	0.010	0.504	0.42
3.5	0.108×10^6	3.63	0.64	0.020	0.504	0.42
4.5	0.108×10^6	4.34	0.48	0.037	0.504	0.42
10.3	0.013×10^6	11.56	0.82	0.813	0.127	0.099
10.3	0.033×10^6	11.63	0.83	0.447	0.285	0.191

TABLE III MAXIMUM WAVE HEATING

Re_∞/cm	M_∞	ϕ (deg)	ϵ = 0.61 cm h_{max}/hFP	ϵ = 0.29 cm h_{max}/hFP
0.013×10^6	10.3	0	1.01	.95
		15	1.7	1.53
		75	1.85	1.55
		90	2.0	1.75
0.033×10^6		0	1.06	1.03
		15	2.3	1.70
		75	2.3	1.90
		90	2.4	2.10
0.108×10^6	2.5	0	.9	1.03
	3.5		.95	.98
	4.5		1.20	1.0
	2.5	7.5	1.4	*
	3.5		1.5	*
	4.5		2.1	*
	2.5	15	1.5	*
	3.5		1.7	*
	4.5		2.4	*
	2.5	30	1.7	1.6
	3.5		1.9	1.8
	4.5		2.5	2.5
	2.5	60	1.9	*
	3.5		2.1	*
	4.5		2.7	*
	2.5	90	2.0	1.9
	3.5		2.3	2.2
	4.5		2.9	2.85

* No Data Taken

TABLE IV AVERAGE WAVE HEATING

Re_∞/cm	M_∞	Ø (deg)	$\varepsilon = 0.61$ cm h_{av}/h_{FP}	$\varepsilon = 0.29$ cm h_{av}/h_{FP}
0.013×10^6	10.3	0	.762	.773
		15	.957	1.01
		75	.899	.923
		90	.959	.980
0.033×10^6		0	1.07	.998
		15	1.35	1.05
		75	1.00	.923
		90	1.04	1.02
0.108×10^6	2.5	0	.758	.956
	3.5		.986	.947
	4.5		1.20	.965
	2.5	7.5	1.04	*
	3.5		1.00	*
	4.5		1.34	*
	2.5	15	1.07	*
	3.5		1.18	*
	4.5		1.54	*
	2.5	30	1.12	1.04
	3.5		1.23	1.06
	4.5		1.49	1.30
	2.5	60	1.24	*
	3.5		1.15	*
	4.5		1.33	*
	2.5	90	1.20	1.19
	3.5		1.31	1.19
	4.5		1.44	1.35

* No Data Taken

TABLE V SURFACE ANGLE AT REATTACHMENT AND MAXIMUM SURFACE ANGLE

Re_∞/cm	M_∞	ϕ, DEG	ε = .61 cm		ε = .29cm	
			SIN α	SIN α_{max}	SIN α	SIN α_{max}
$.013X10^6$	10.3	15	.087	.41	.056	.105
		75	.303	.858	.225	.365
		90	.259	.866	.292	.376
$.033X10^6$		15	.087	.410	.063	.105
		75	.303	.858	.225	.365
		90	.334	.866	.259	.376
$.108X10^6$	2.5	7.5	.099	.22	*	*
		15	.208	.41	*	*
		30	.357	.655	.365	.199
		60	.599	.832	*	*
		90	.643	.866	.375	.376
	3.5	7.5	.083	.22	*	*
		15	.195	.41	*	*
		30	.357	.655	.365	.199
		60	.599	.832	*	*
		90	.629	.866	.375	.376
	4.5	7.5	.099	.22	*	*
		15	.195	.41	*	*
		30	.357	.655	.365	.199
		60	.599	.832	*	*
		90	.643	.866	.375	.376

* NO DATA TAKEN

TABLE VI FLOW CONDITIONS AND DATA FROM OTHER SOURCES

REFERENCE	ε/L	M_∞	Re_∞/cm	Tw/T_{T_∞}	δ^*,cm	θ, cm	s in α	h_{max}/h_{FP}
(1)	.055	3	.46	.55	.42	.11	.265	2.06
	.046						.219	1.87
	.045						.238	1.82
	.041						.211	1.75
	.026						.146	1.55
(2)	.043	3.51	.13	.81	3.63	.64	.145	1.30
(3)	.029	6.67	.119	.3	.254	.020	.180	2.0
	.032				.254	.020	.197	3.3
	.050				.254	.020	.299	3.5
	.067				.254	.020	.388	5.1
(4)	.085	4	$.386 \times 10^6$	.6	.126	.020	.471	4.0
			.201		.142	.022		4.1
			.091		.176	.028		4.35
		6	.272		.211	.0156		5.7
			.142		.241	.0179		6.7
			.063		.297	.0223		7.6
	.043		.272		.211	.0156	.258	3.1
			.142		.241	.0179		3.6
			.063		.297	.0223		4.1
	.021		.272		.211	.0156	.131	2.1
			.142		.241	.0179		2.4
			.063		.297	.0223		2.6
	.067	4	.386		.063	.0098	.388	3.2
			.244		.068	.0106		3.5
			.126		.085	.0133		3.9
		6	.272		.115	.0085		5.1
			.169		.130	.0096		5.9
(5)	.034	6.9	.52	.4	.018	.0012	.206	4.0
		5.8	.37		.053	.0049		4.0

TABLE VII COMPARISON OF AVERAGE HEATING WITH DIRLING'S PREDICTIONS

M_∞	Re_∞/cm	ε(cm)	ϕ(DEG)	h_{av}/h_{FP} MEAS	h_{av}/h_{FP} PRED
2.5	$.108 \times 10^6$	.29	90	1.19	1.29
2.5		.61		1.20	1.48
3.5		.29		1.19	1.23
3.5		.61		1.31	1.38
4.5		.29		1.35	1.14
4.5		.61		1.44	1.37
10.3	$.013 \times 10^6$	.29		.98	1.00
	$.013 \times 10^6$	.61		.959	.93
	$.033 \times 10^6$	.29		1.02	1.00
	$.033 \times 10^6$	.61		1.04	1.04

TABLE VII COMPARISON OF AVERAGE HEATING WITH DIRLING'S PREDICTIONS

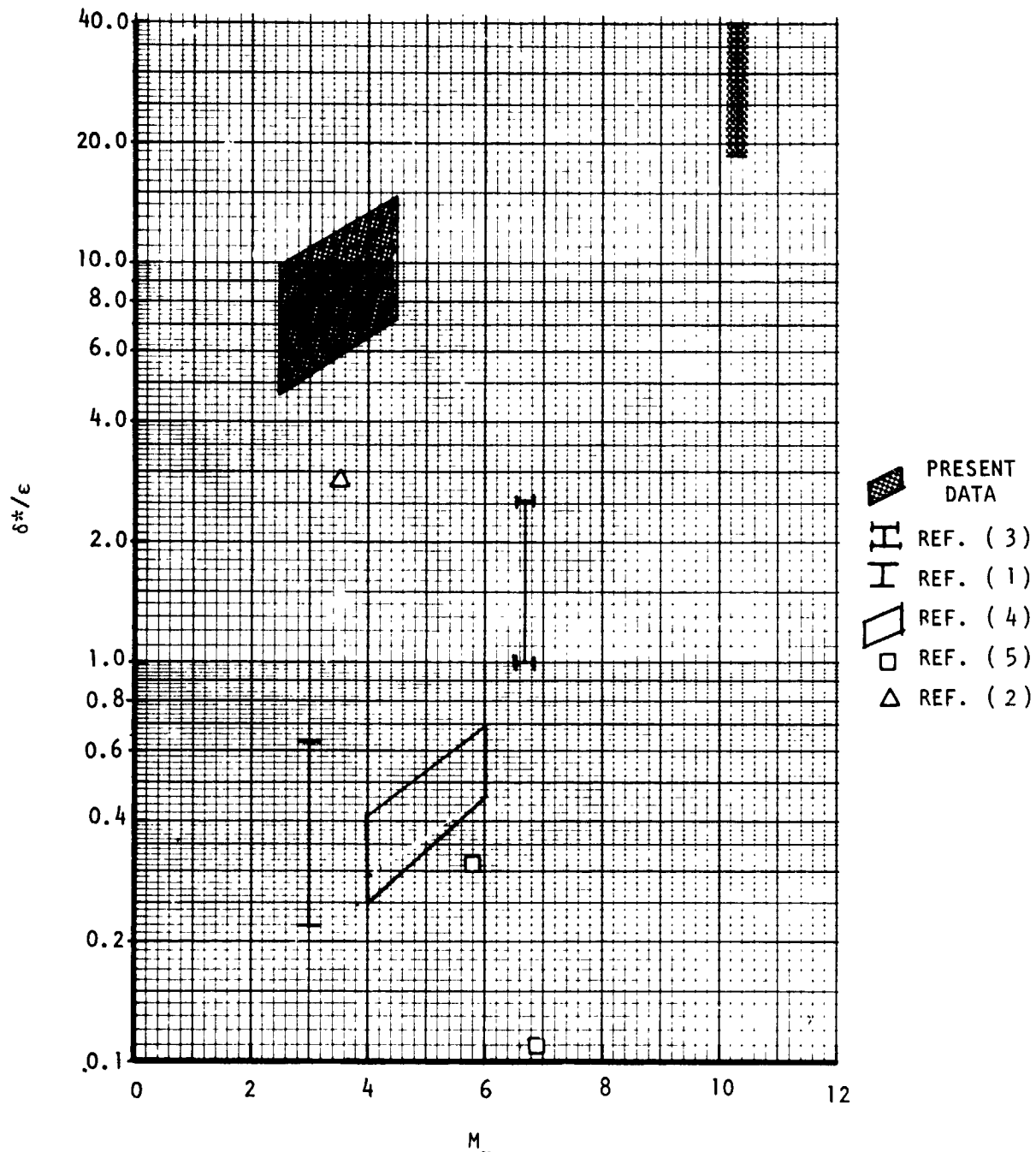

FIGURE 1 - COMPARISON OF TURBULENT HEATING DATA

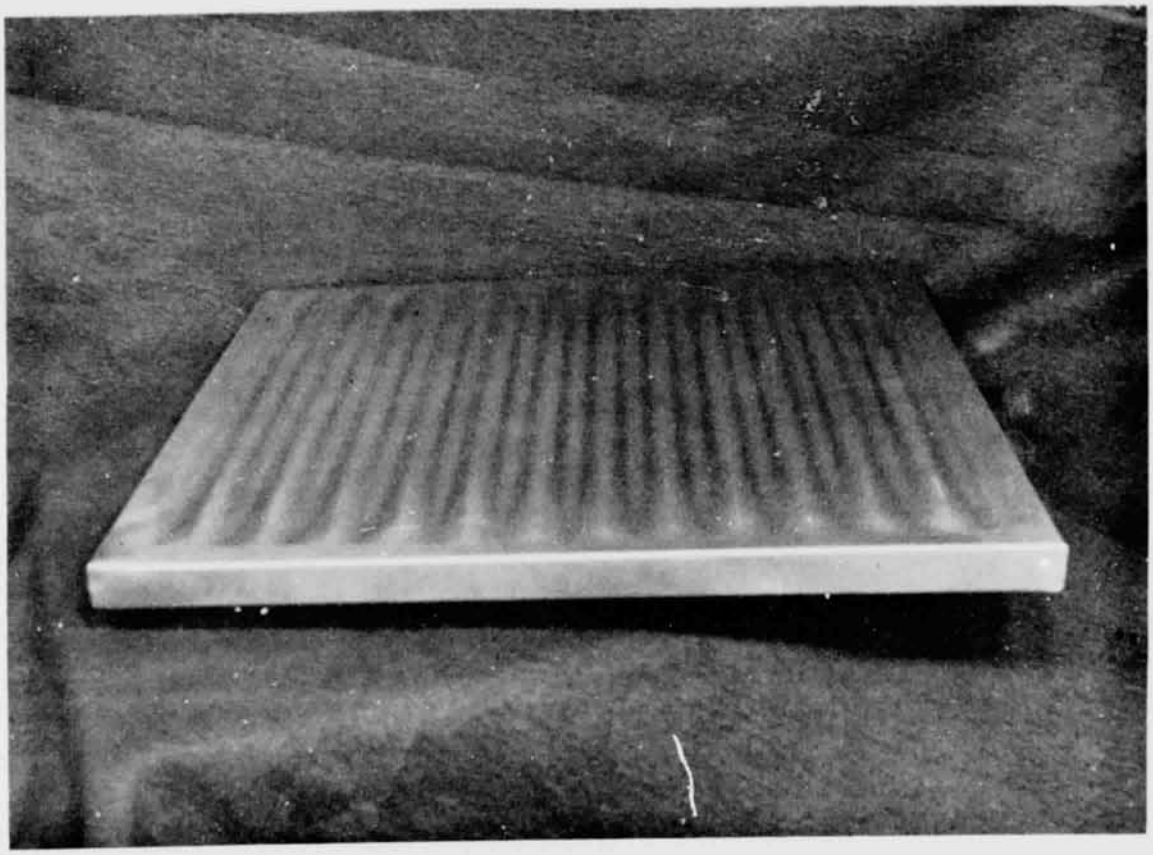

FIGURE 2 PHOTOGRAPH OF BEADED PANEL, WAVE HEIGHT = 0.61 cm

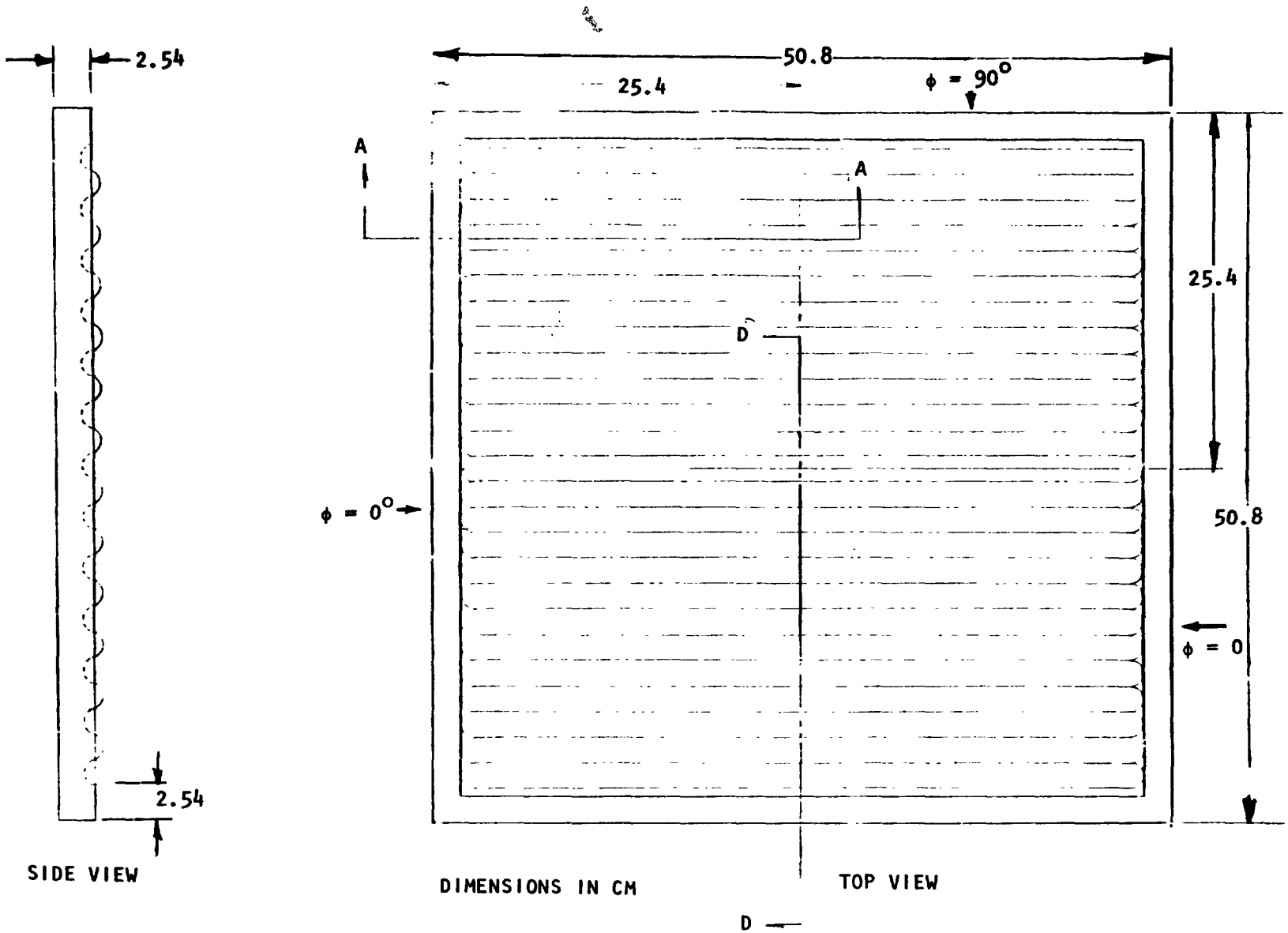

FIGURE 3- A) PANEL CONFIGURATION - TOP AND SIDE VIEWS

NOTE: -1 DIMENSION FOR LARGER CORRUGATION HEIGHT

-3 DIMENSION FOR SMALLER CORRUGATION HEIGHT

DIMENSIONS IN CM

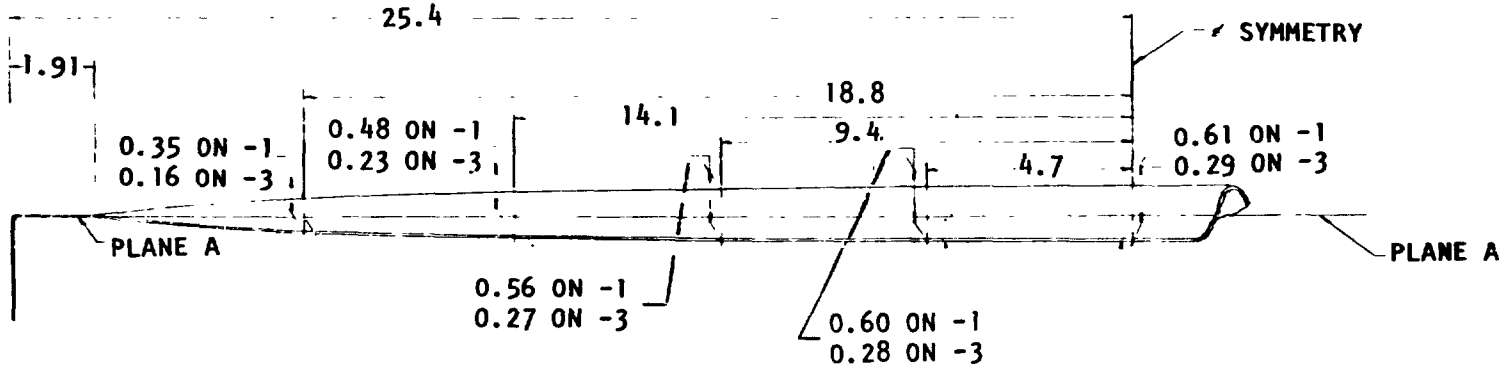

A-A

FIGURE 3- B) PANEL CONFIGURATION - CORRUGATION SHAPE FOR $\phi = 0^{o}$

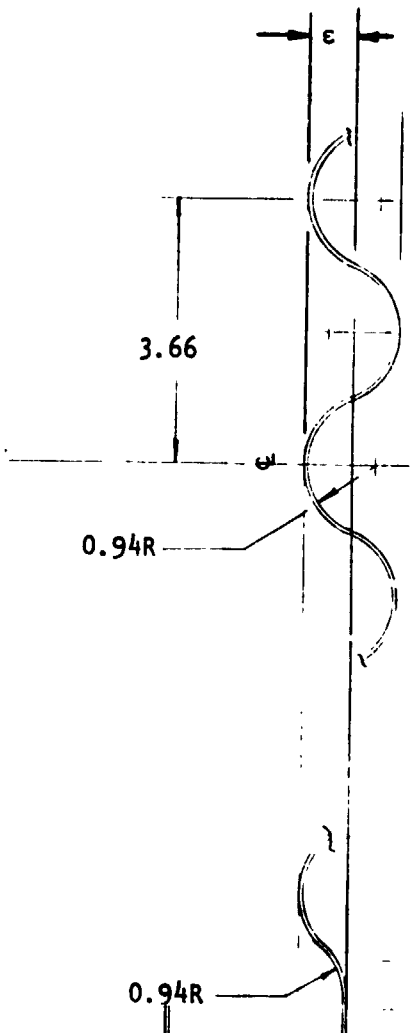

FIGURE 3-C) PANEL CONFIGURATION - CORRUGATION SHAPE FOR $\phi = 90^{\circ}$

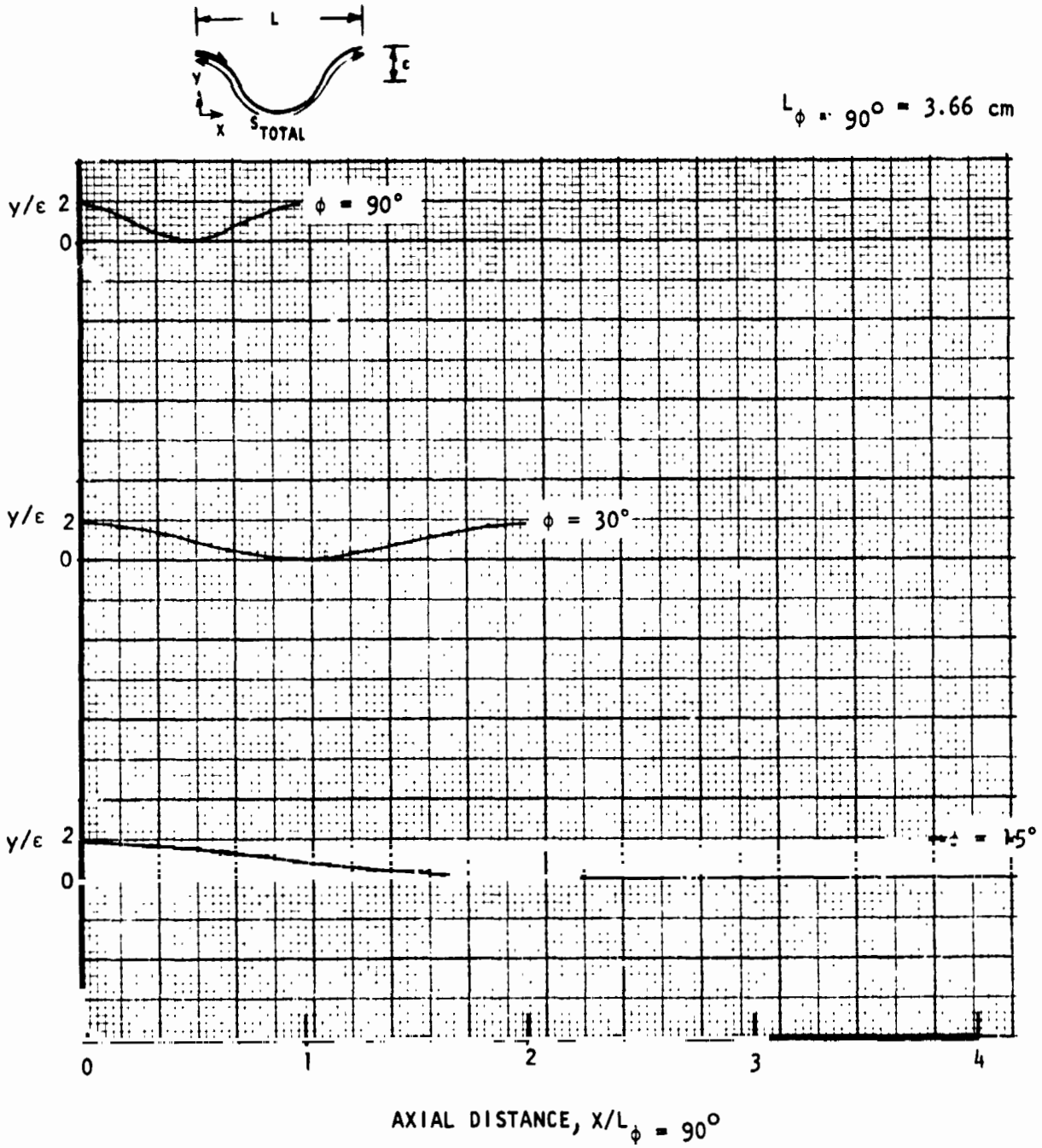

FIGURE 4 - WAVE SHAPE AS A FUNCTION OF THE FLOW ANGLE, ε = 0.29 cm

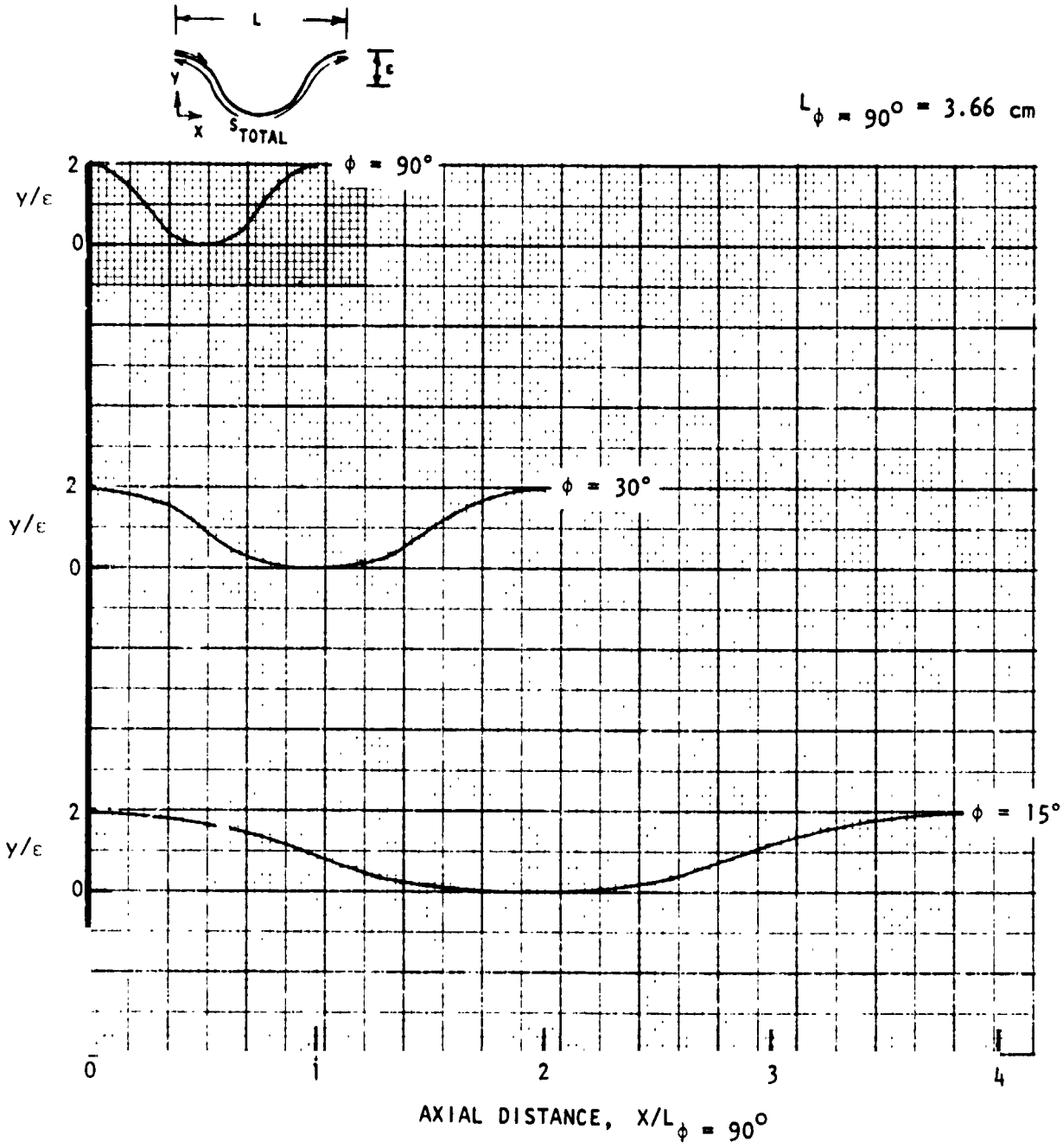

FIGURE 5 - WAVE SHAPE AS A FUNCTION OF THE FLOW ANGLE, $\varepsilon = 0.61$ cm

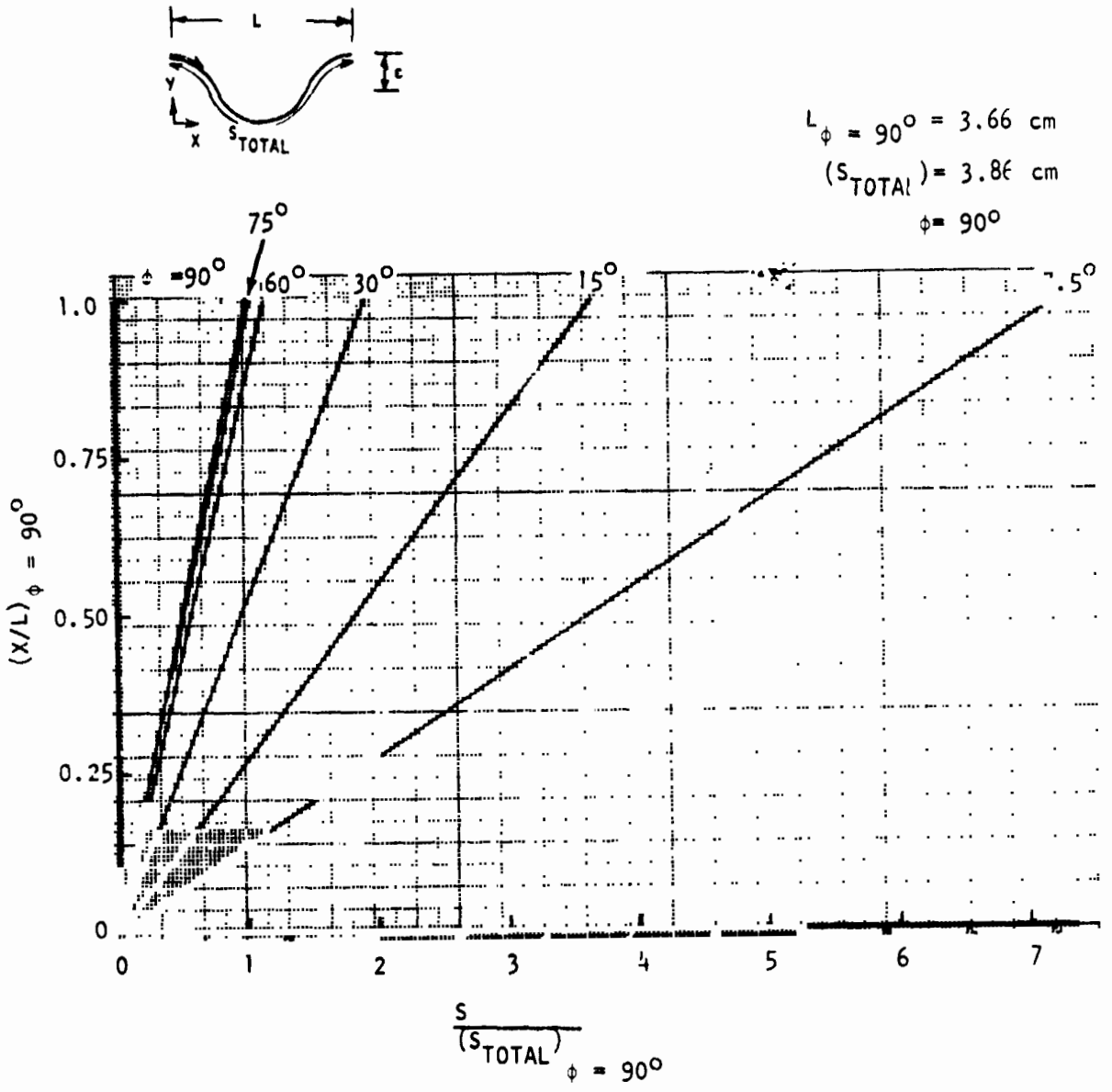

FIGURE 6 - SURFACE DISTANCE AS A FUNCTION OF THE FLOW ANGLE, c = 0.29 cm

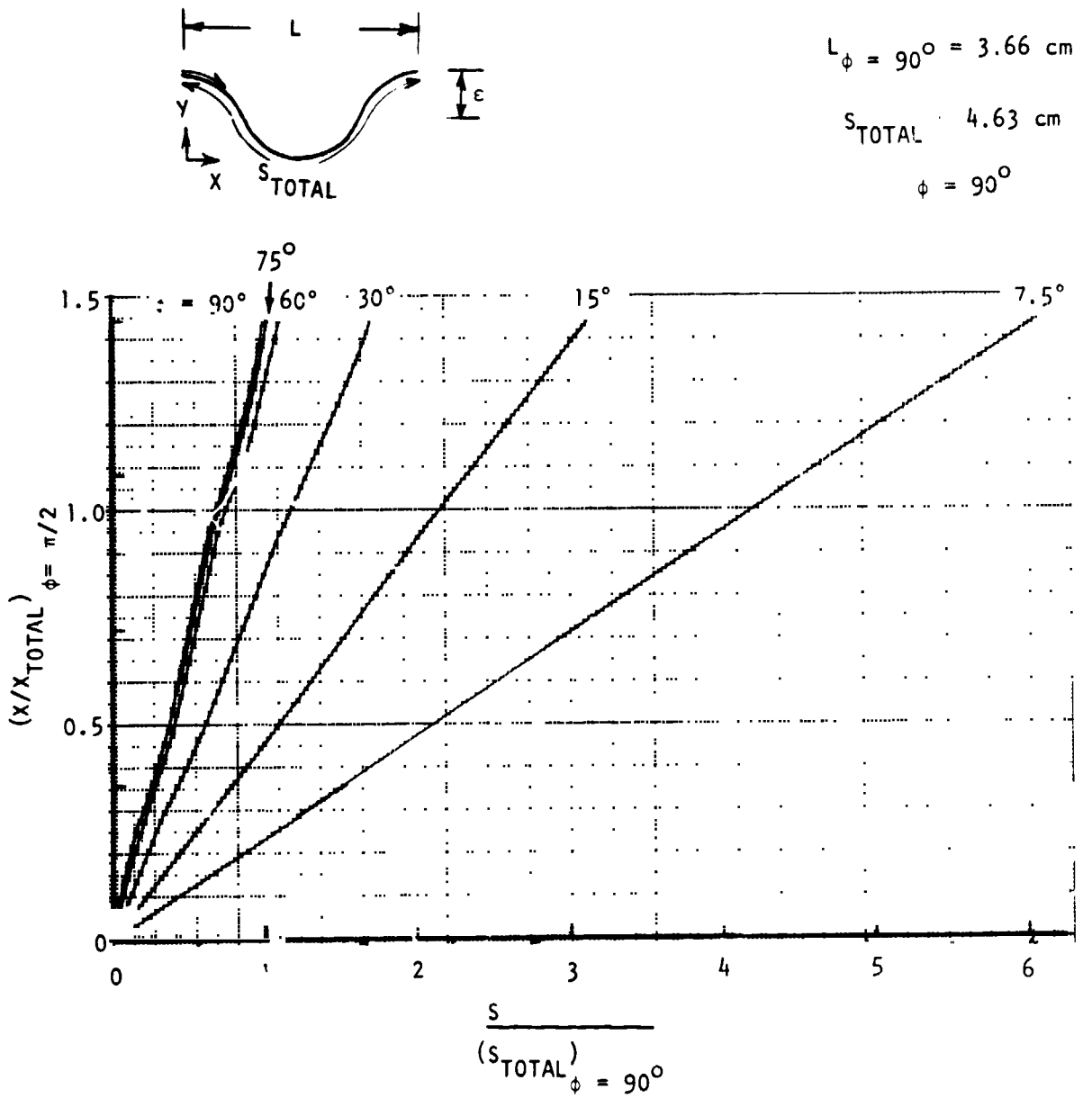

FIGURE 7 - SURFACE DISTANCE AS A FUNCTION OF THE FLOW ANGLE, ε = 0.61 cm

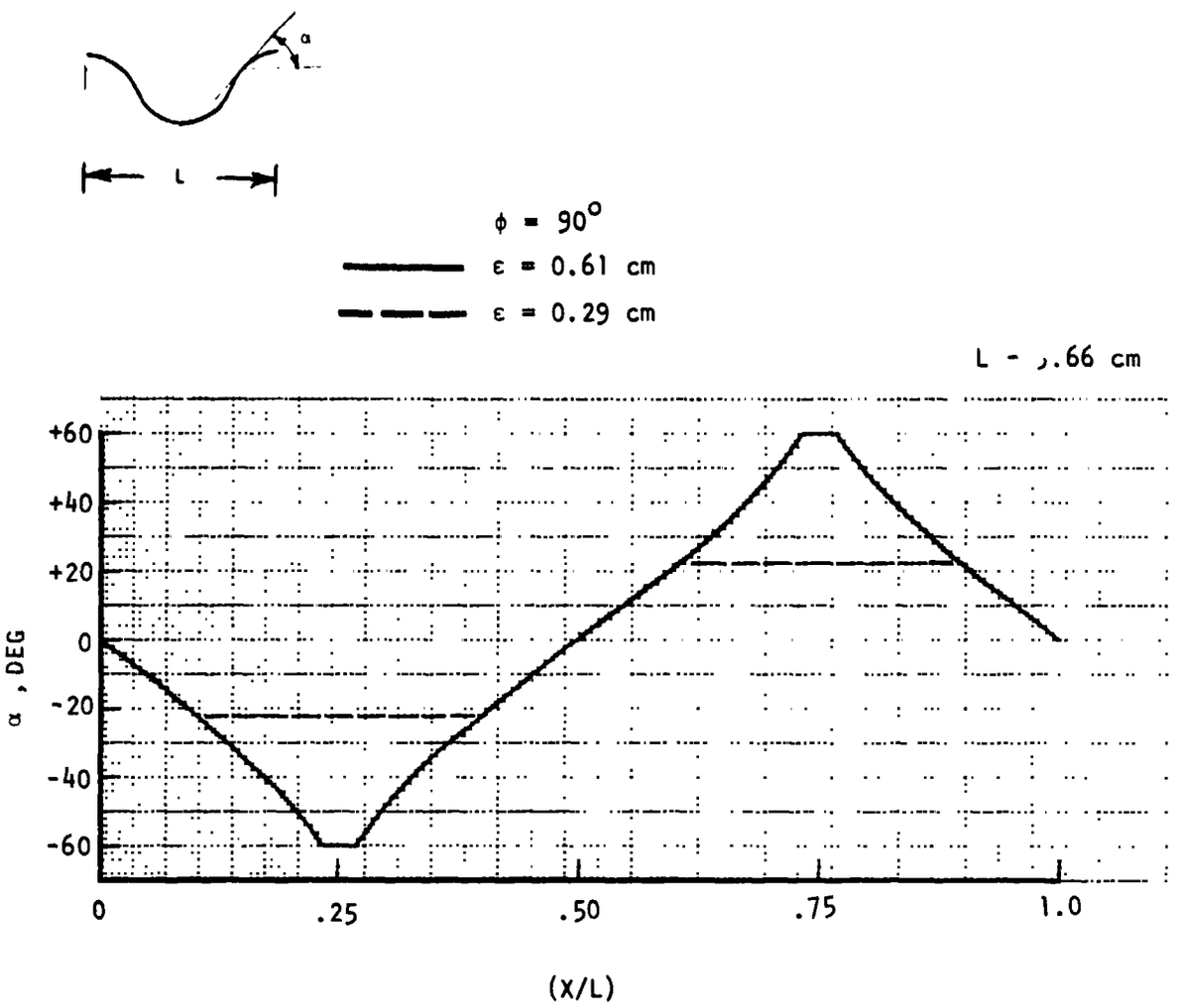

FIGURE 8 - LOCAL SURFACE ANGLE

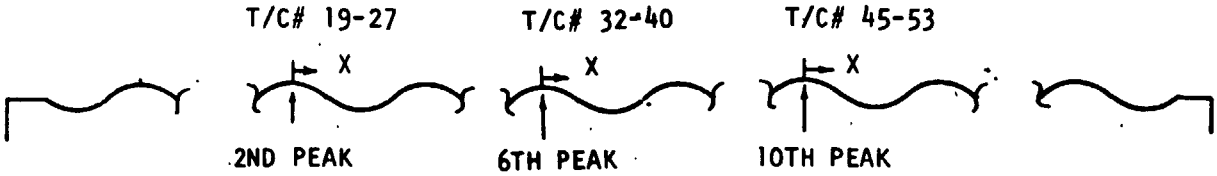

TC#	X(cm)	TC#	X(cm)	TC#	X(cm)
19	0.020	32	0.404	45	0.013
20	0.396	33	0.787	46	0.467
21	0.927	34	1.047	47	0.935
22	1.339	35	1.283	48	1.369
23	1.709	36	1.798	49	1.829
24	2.286	37	2.286	50	2.332
25	2.784	38	2.718	51	2.753
26	3.279	39	3.183	52	3.195
27	3.703	40	3.602	53	3.668

FIGURE 9 - THERMOCOUPLE LOCATIONS, ε = 0.29 cm

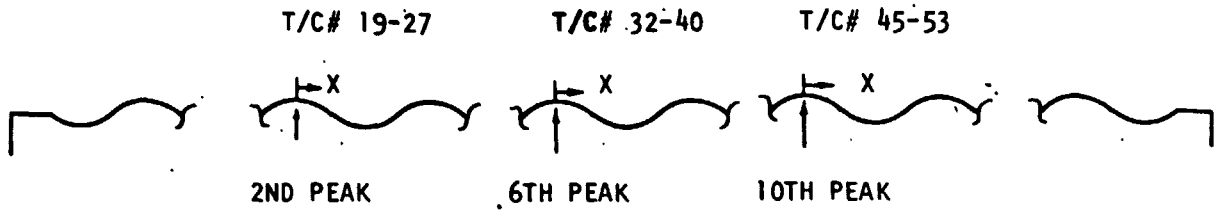

TC#	X(cm)	TC#	X(cm)	TC#	X(cm)
19	-0.046	32	0.005	45	0.031
20	0.536	33	0.582	46	0.452
21	0.978	34	1.054	47	0.937
22	1.318	35	1.428	48	1.415
23	1.829	36	1.829	49	1.768
24	2.314	37	2.286	50	2.324
25	2.687	38	2.769	51	2.690
26	3.216	39	3.226	52	3.165
27	2.693	40	3.680	53	3.675

FIGURE 10 - THERMOCOUPLE LOCATIONS, $\epsilon = 0.61$ cm

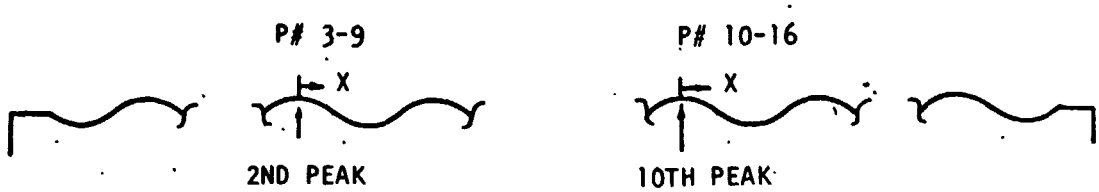

P#	UPWT TEST X(cm)	CFHT TEST X(cm)
3	-0.056	-0.081
4	0.622	0.587
5	1.161	1.092
6	1.821	1.803
7	2.451	2.487
8	3.038	3.112
9	3.625	3.584

P#	X(cm)
10	-0.028
11	0.566
12	1.232
13	1.809
14	2.377
15	3.005
16	3.569

FIGURE 11 - PRESSURE TAP LOCATIONS, $\varepsilon = 0.29$ cm

P#. 3-9

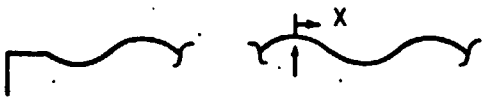

2ND PEAK

P# 10-16

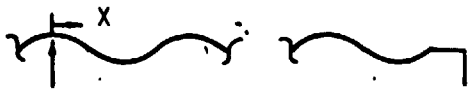

10TH PEAK

P#	X(cm)
3	-0.051
4	0.627
5	1.163
6	1.847
7	2.507
8	3.030
9	3.640

P#	X(cm)
10	0
11	0.676
12	1.214
13	1.801
14	2.461
15	2.921
16	3.686

FIGURE 12 - PRESSURE TAP LOCATIONS, ε = 0.61 cm

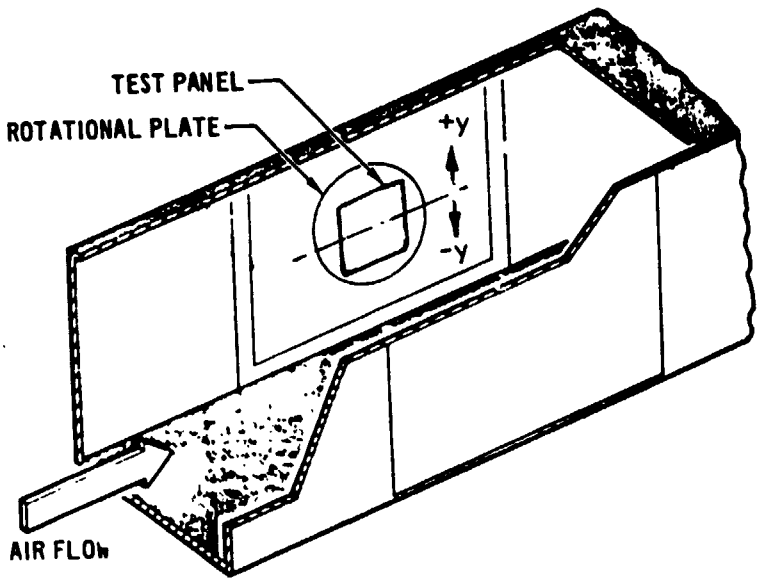

FIGURE 13 - MODEL INSTALLATION

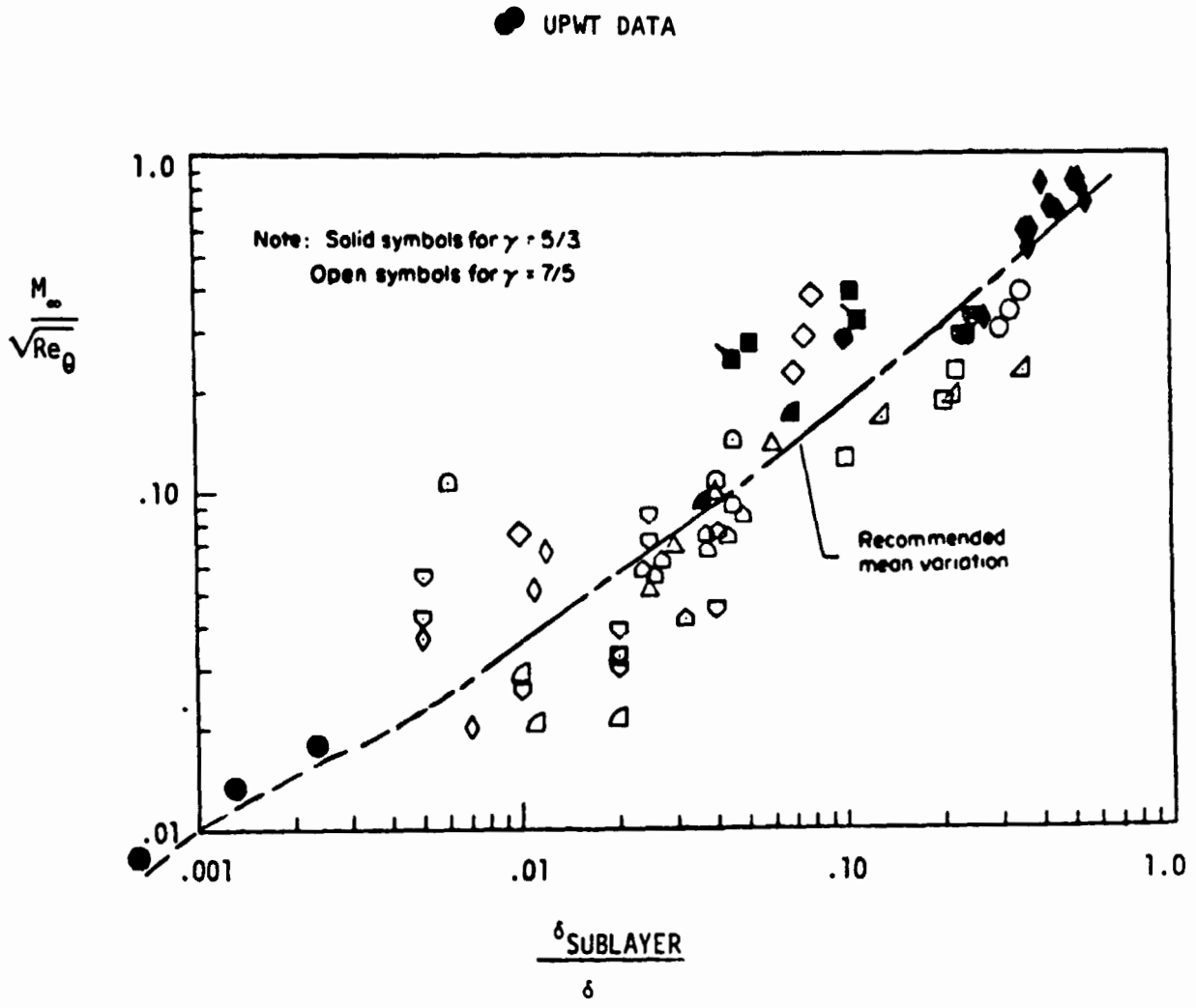

FIGURE 14 - LAMINAR SUBLAYER THICKNESS FOR NOZZLE WALL BOUNDARY LAYERS

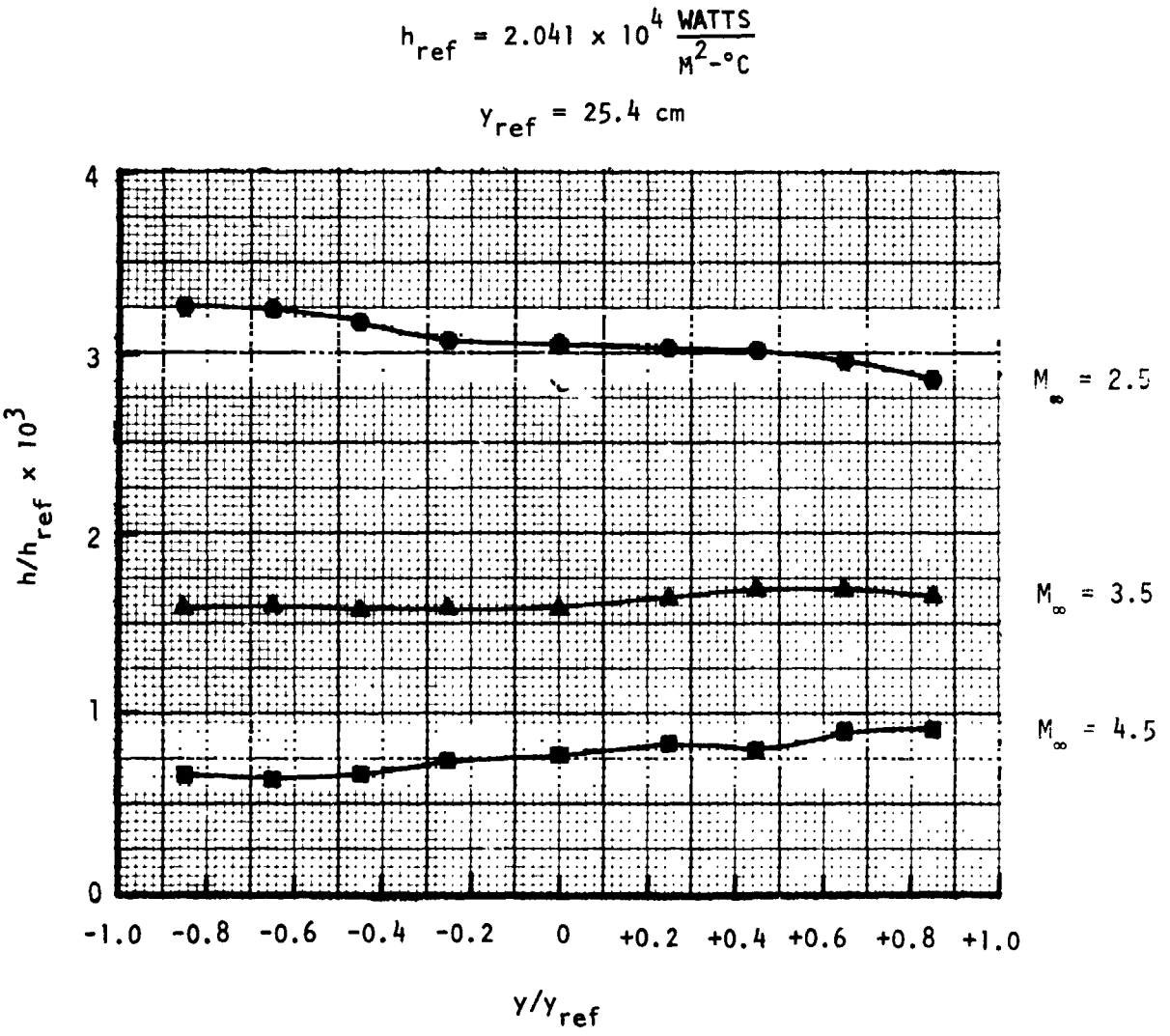

FIGURE 15 - EXPERIMENTAL SPANWISE HEATING DISTRIBUTION ON THE UPWT SIDE WALL

$$h_{ref} = 2.041 \times 10^4 \frac{\text{WATTS}}{M^2\text{-}^\circ C}$$

$$Y_{ref} = 25.4 \text{ cm}$$

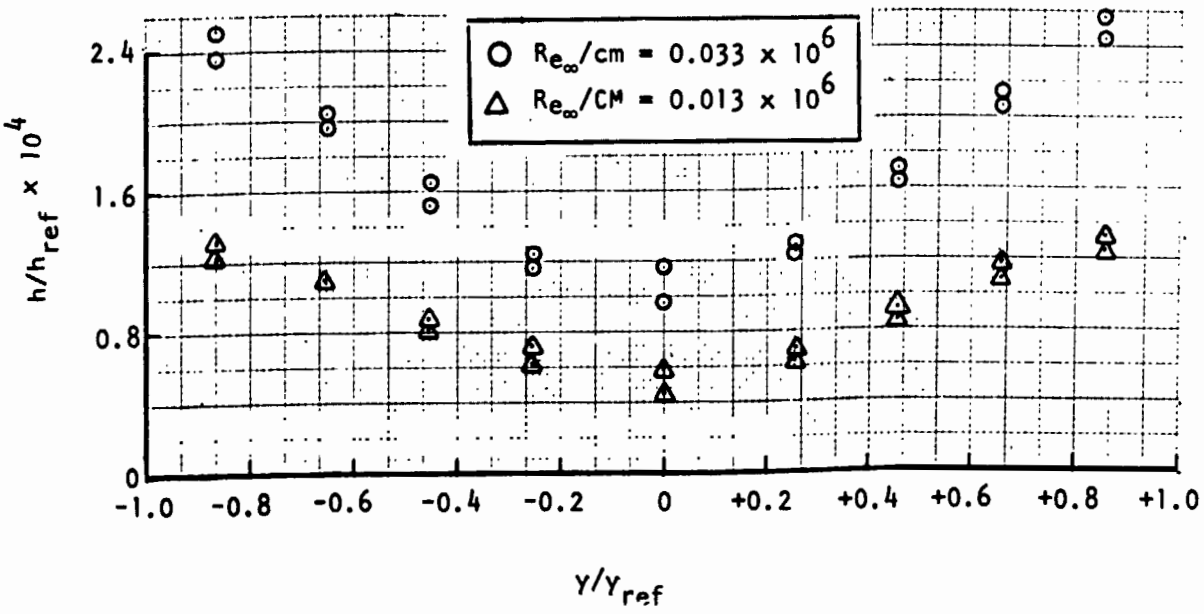

FIGURE 16 - EXPERIMENTAL SPANWISE HEATING DISTRIBUTION ON THE CFHT SIDE WALL, $M_\infty = 10.3$

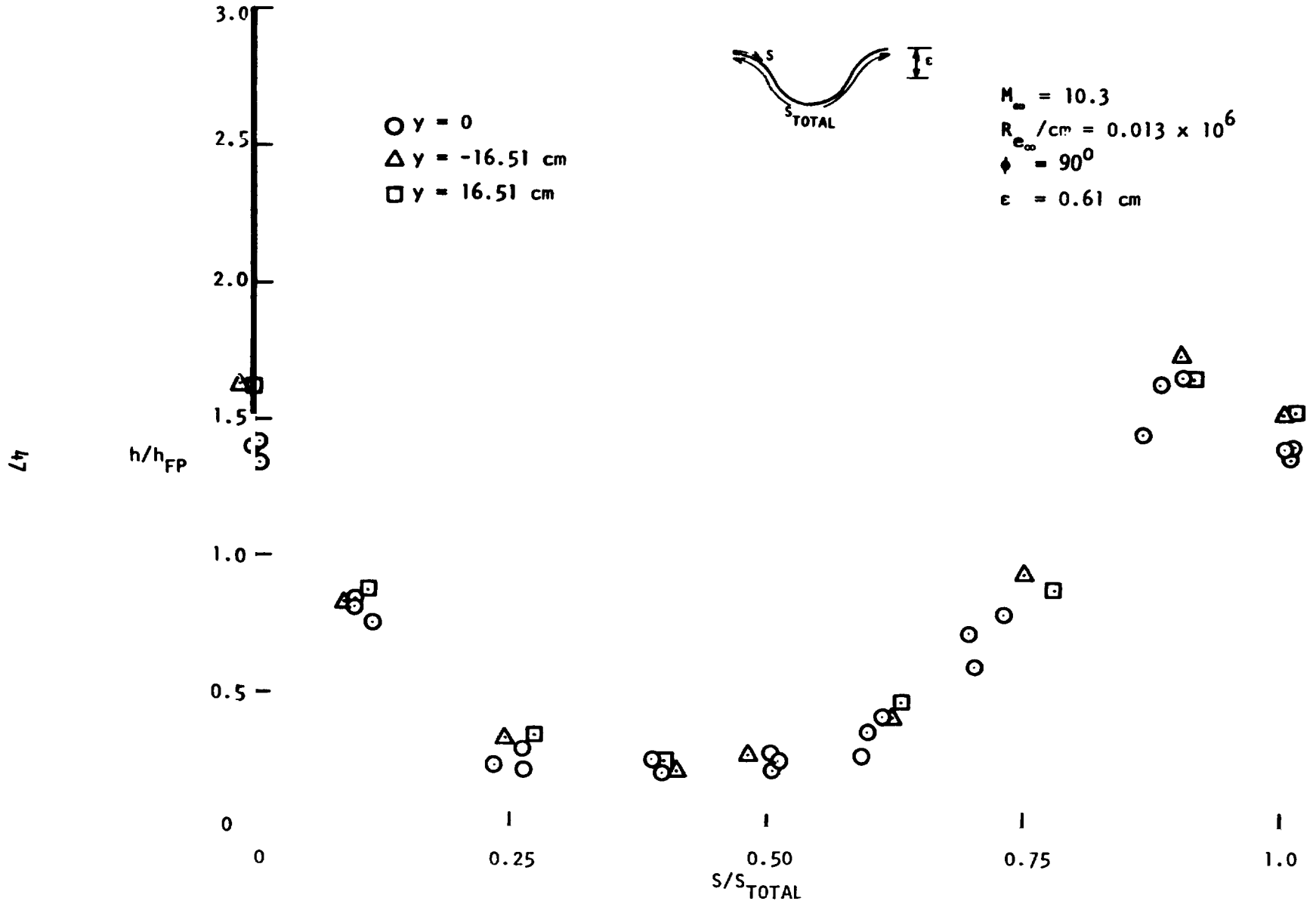

FIGURE 17 - NONDIMENSIONALIZED HEATING DISTRIBUTION

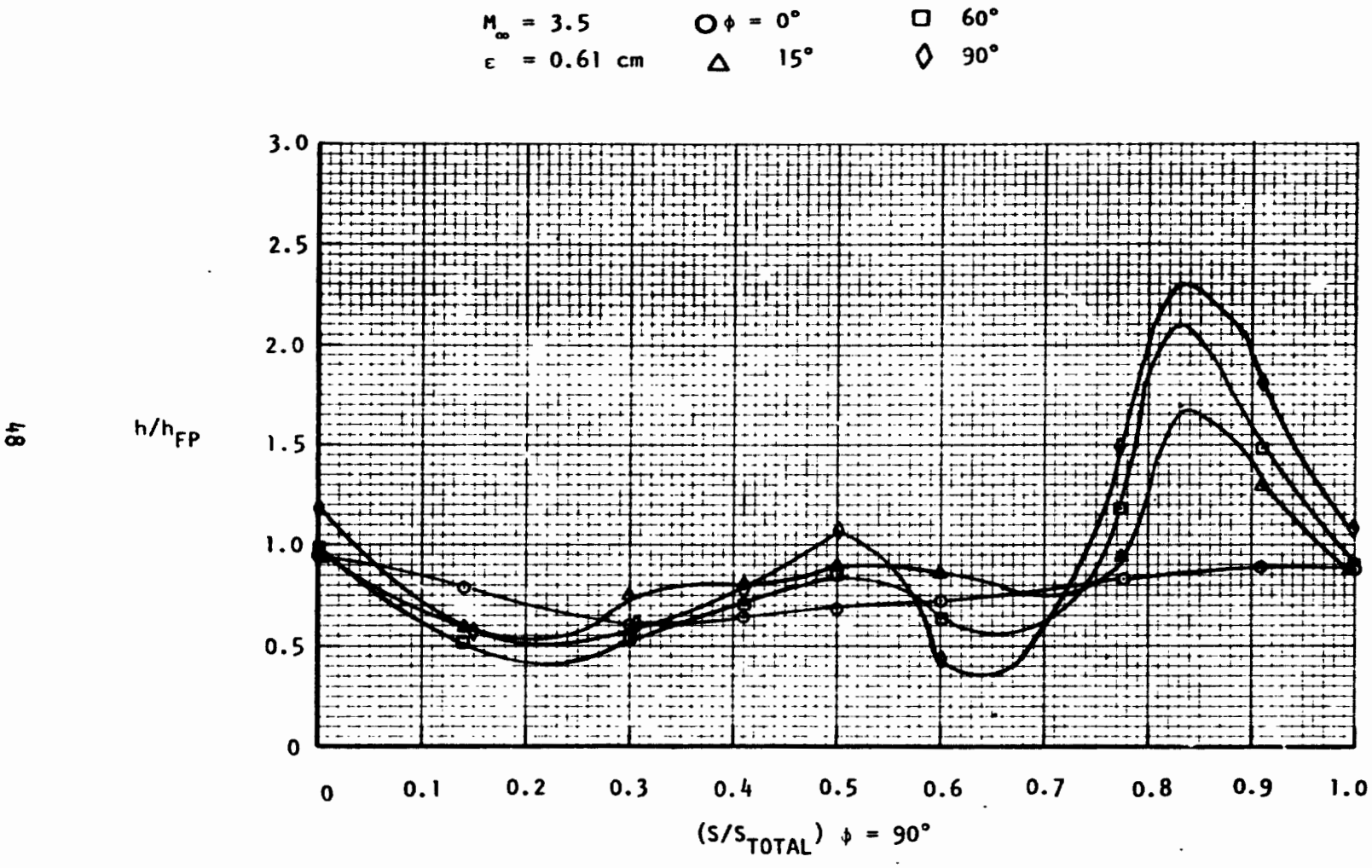

FIGURE 18A - EFFECT OF FLOW ANGLE ON HEATING DISTRIBUTION

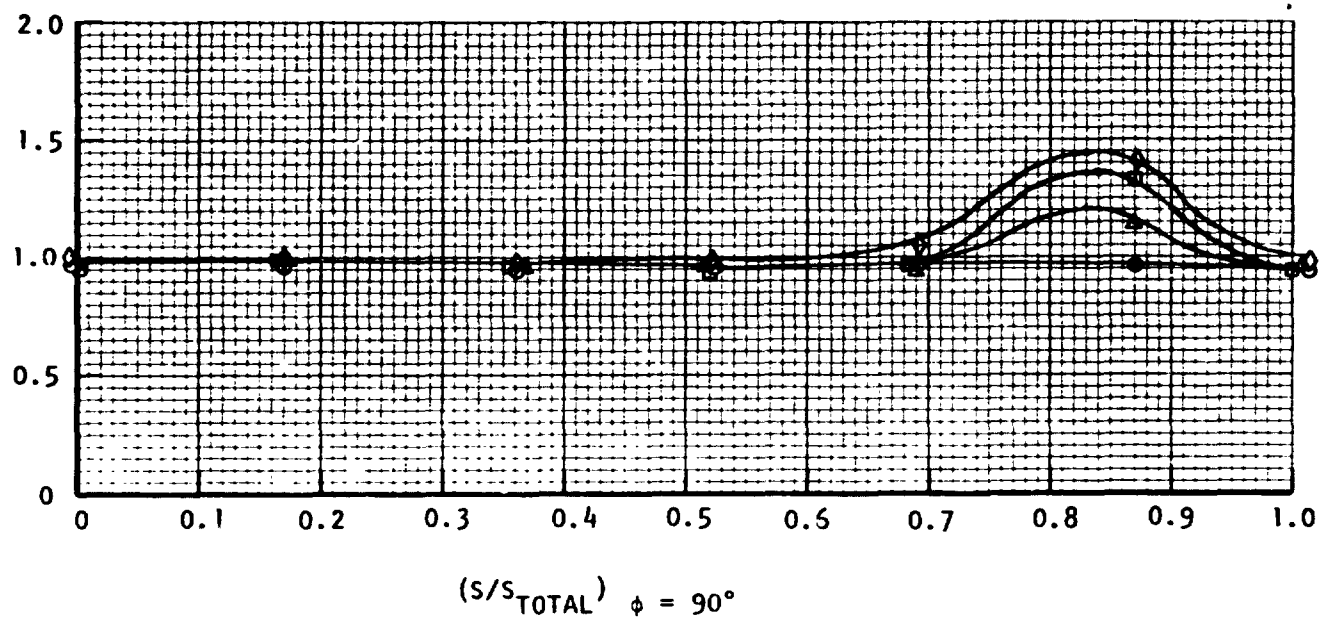

FIGURE 18B - EFFECT OF FLOW ANGLE ON PRESSURE DISTRIBUTION

$M_\infty = 10.3$

$Re_\infty/cm = 0.033 \times 10^6$

$\epsilon = 0.61$ cm

○ $\phi = 0°$
△ 15°
□ 75°
◇ 90°

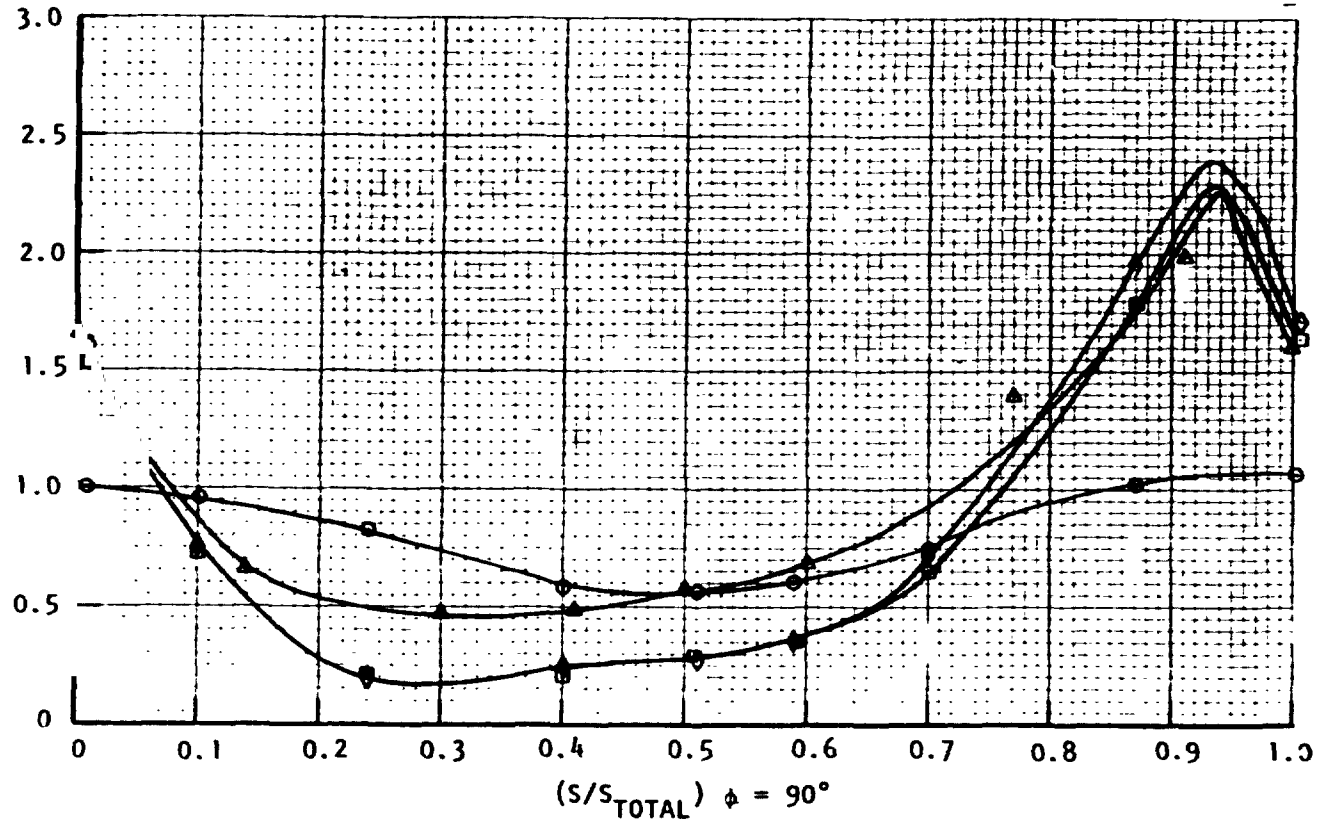

FIGURE 19A - EFFECT OF FLOW ANGLE ON HEATING DISTRIBUTION

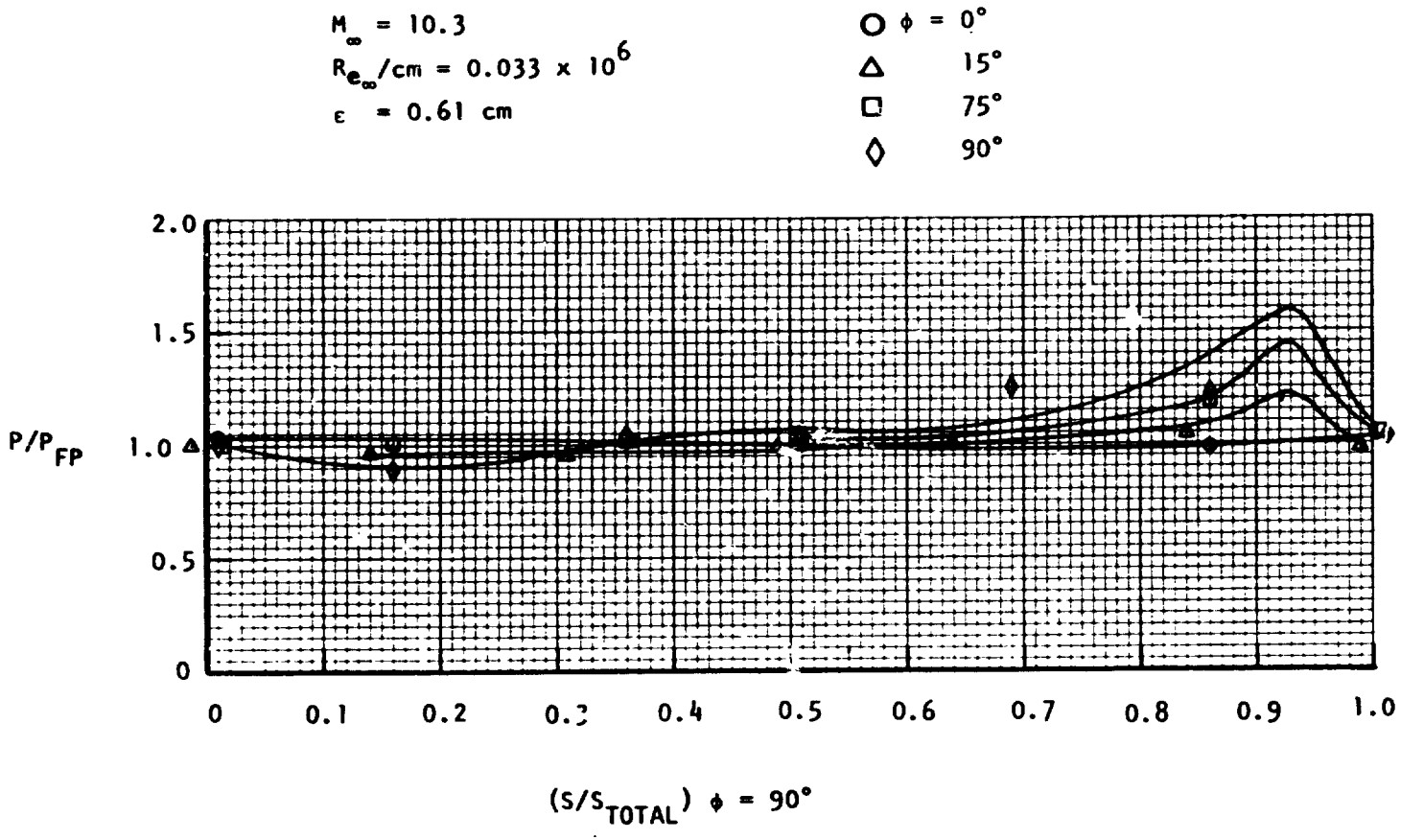

FIGURE 19B - EFFECT OF FLOW ANGLE ON PRESSURE DISTRIBUTION

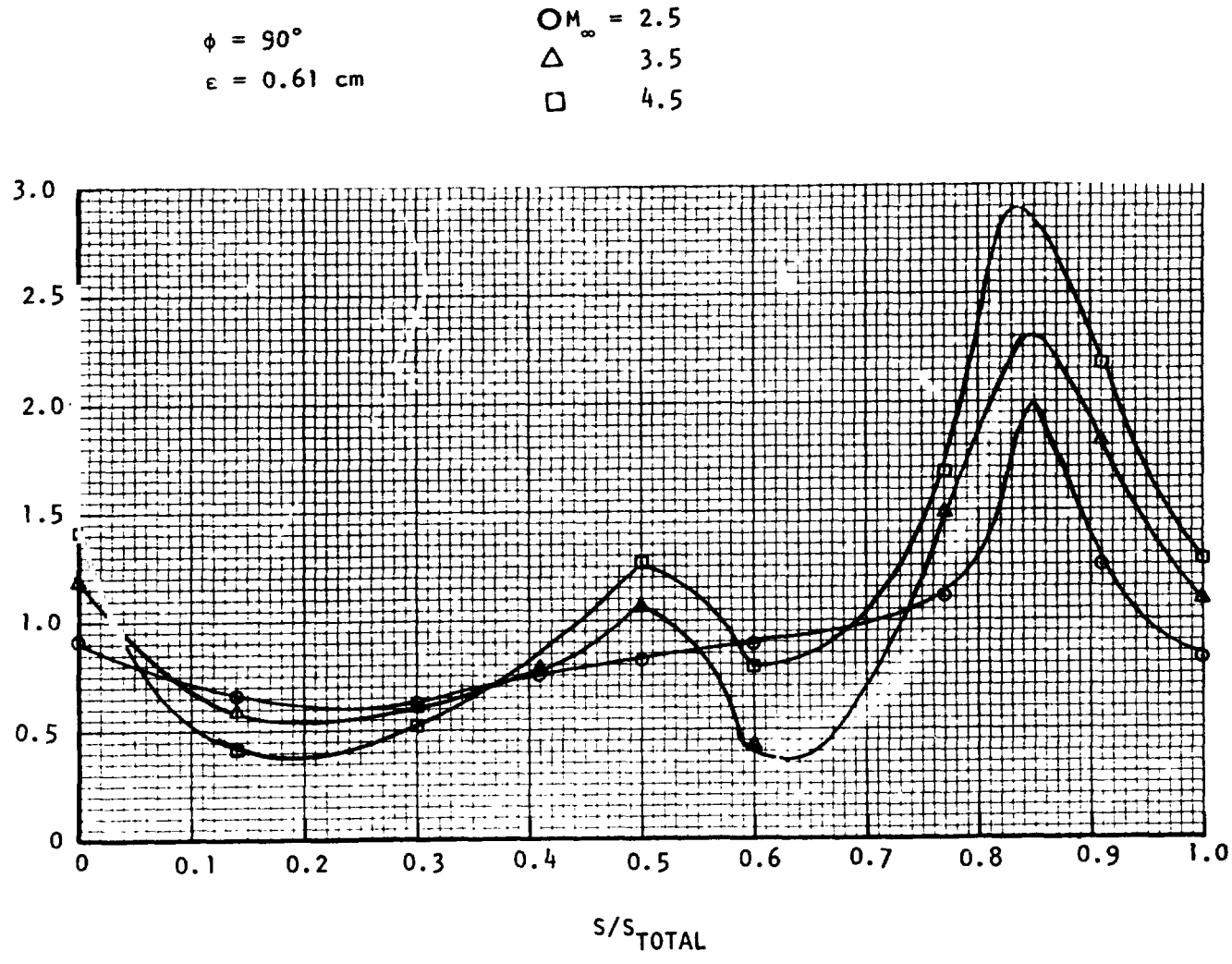

FIGURE 20A - EFFECT OF MACH NUMBER ON HEATING DISTRIBUTION

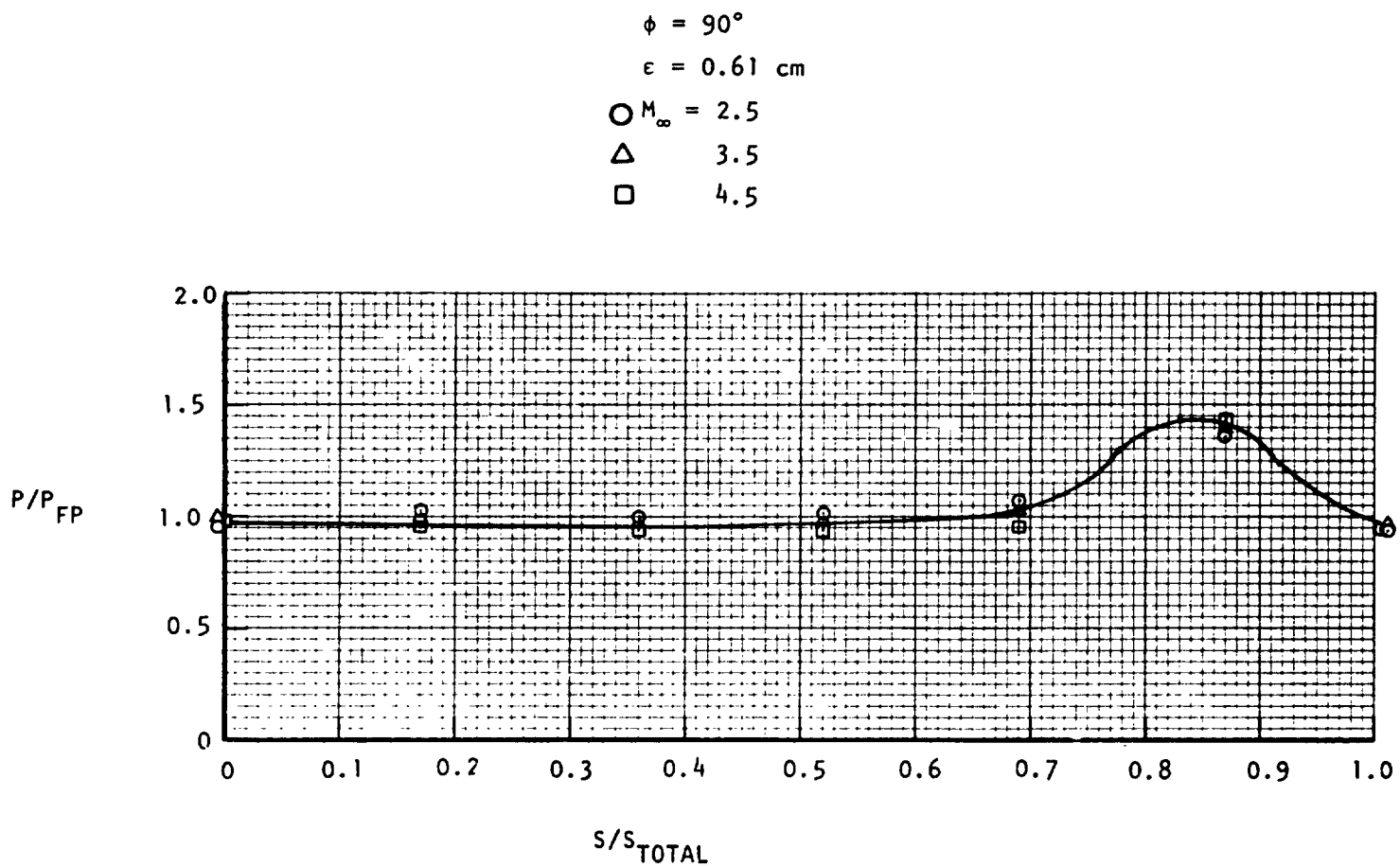

FIGURE 20B - EFFECT OF MACH NUMBER ON PRESSURE DISTRIBUTION

M_∞ = 10.3

γ = 90°

ε = 0.61 cm

○ R_{e_∞}/cm = 0.033 × 10^6

△ R_{e_∞}/cm = 0.013 × 10^6

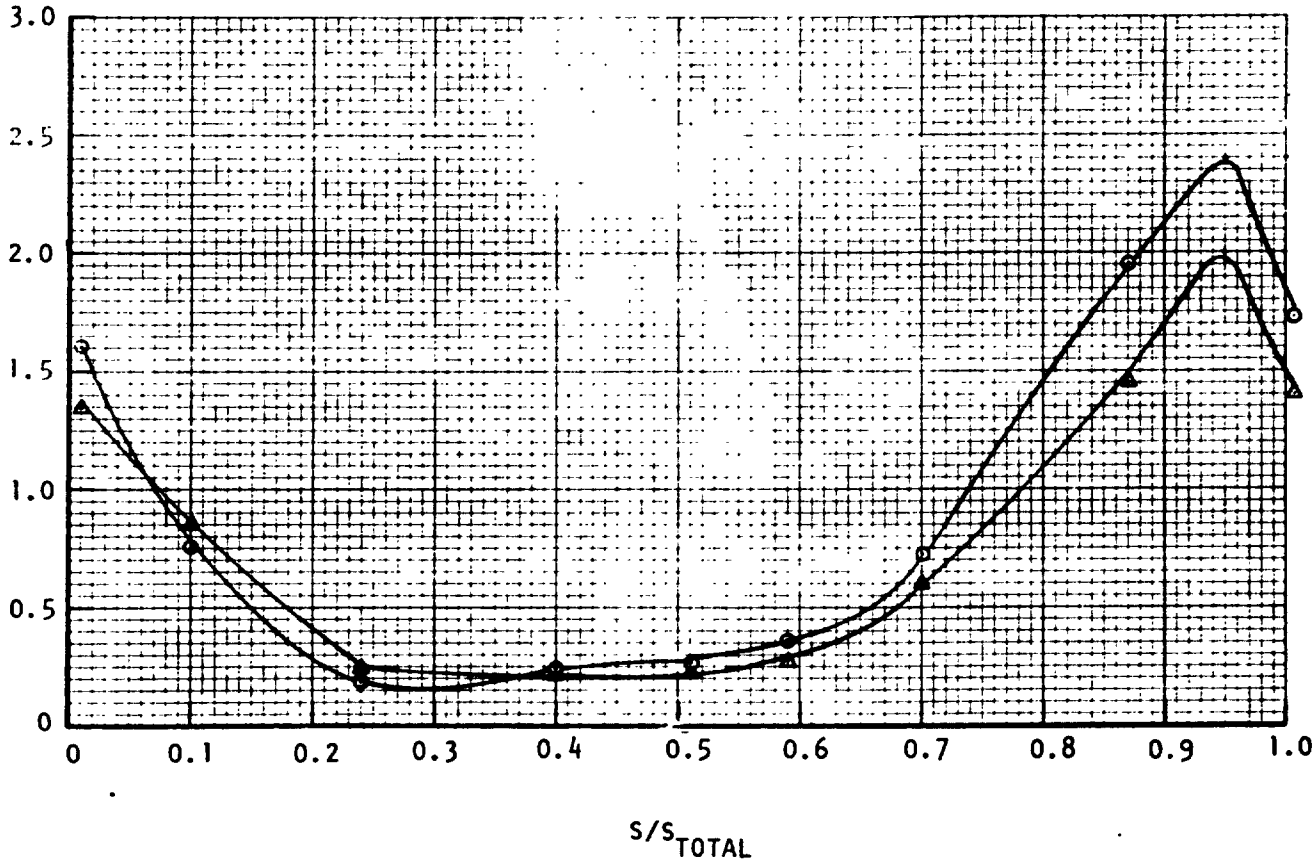

FIGURE 21A - EFFECT OF REYNOLDS NUMBER ON HEATING DISTRIBUTION

$M_\infty = 10.3$

$\varepsilon = 0.61$ cm

O $R_{e_\infty}/cm = 0.033 \times 10^6$

Δ $R_{e_\infty}/cm = 0.013 \times 10^6$

$\phi = 90°$

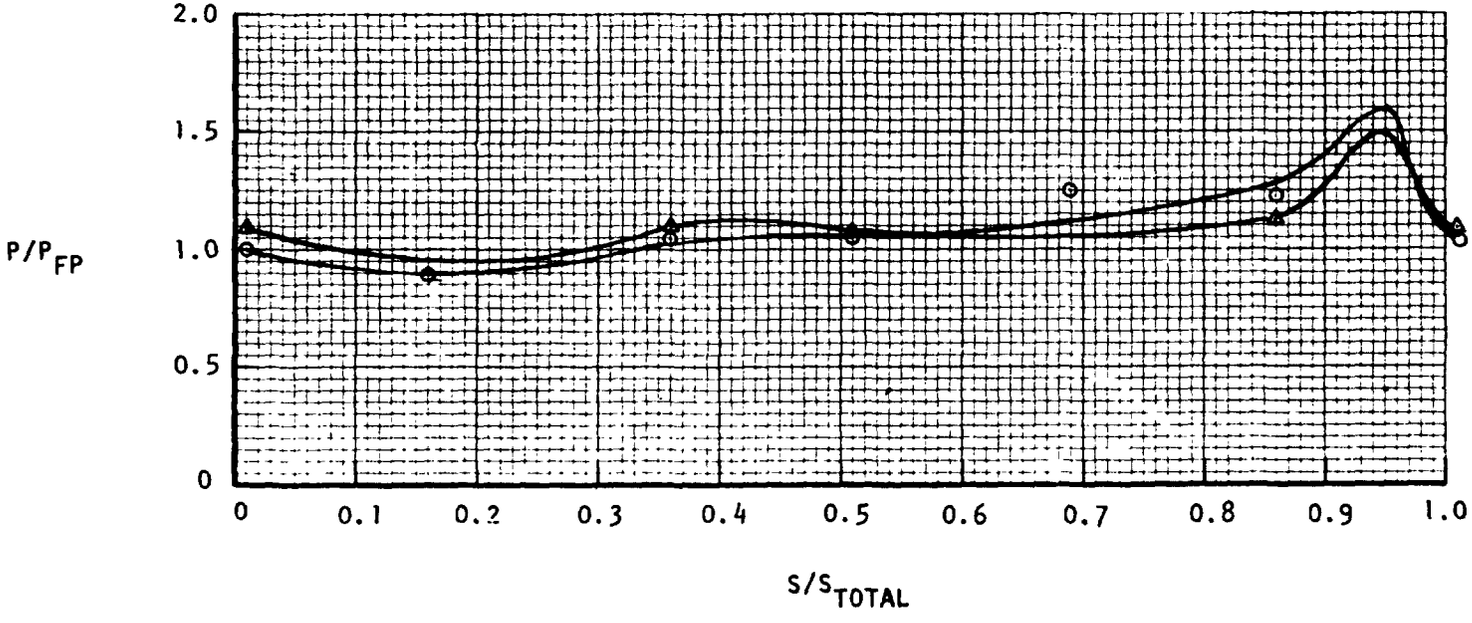

FIGURE 21B - EFFECT OF REYNOLDS NUMBER ON PRESSURE DISTRIBUTION

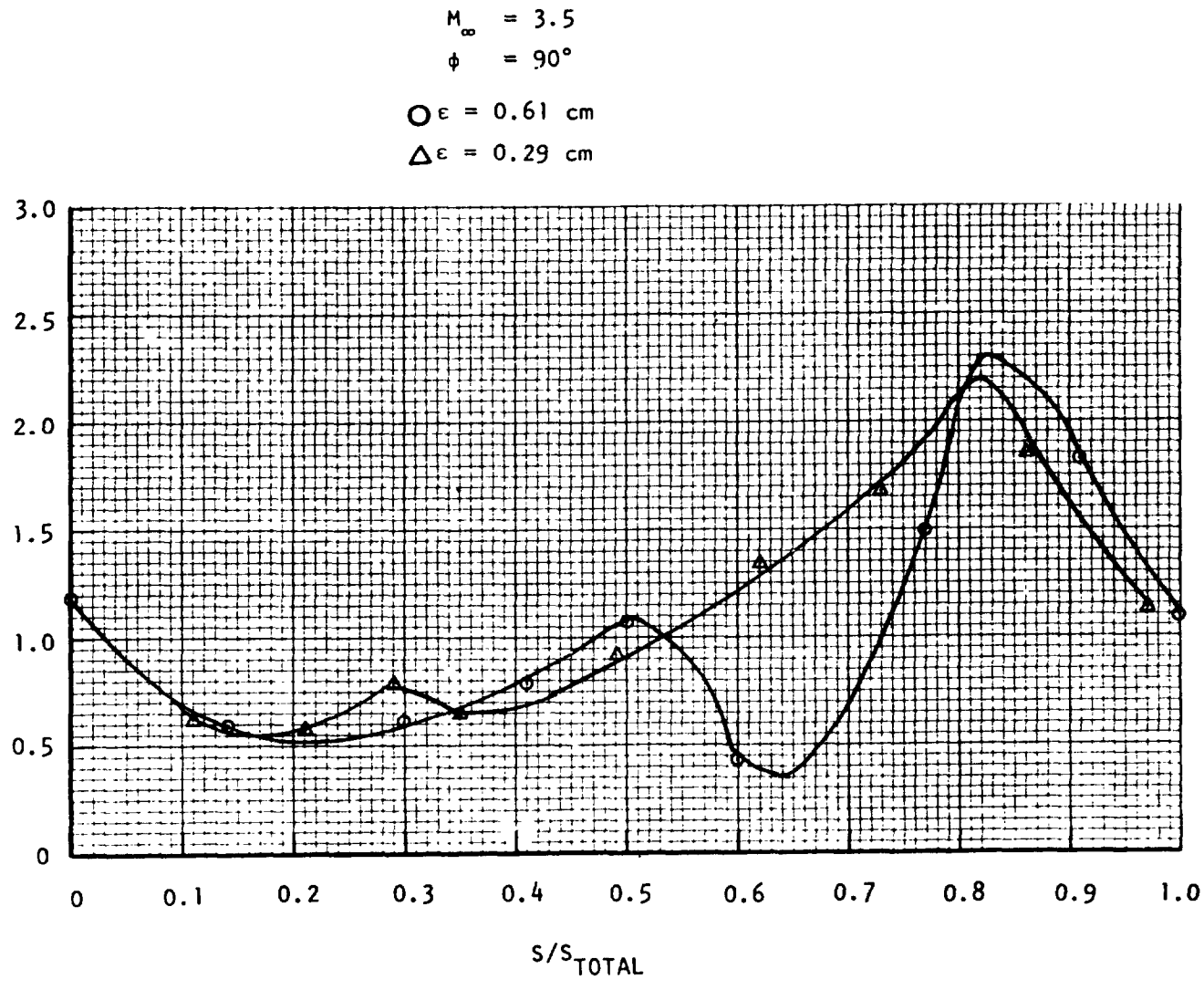

FIGURE 22A - EFFECT OF WAVE HEIGHT ON HEATING DISTRIBUTION

$M_\infty = 3.5$

$\phi = 90°$

○ $\epsilon = 0.61$ cm

△ $\epsilon = 0.29$ cm

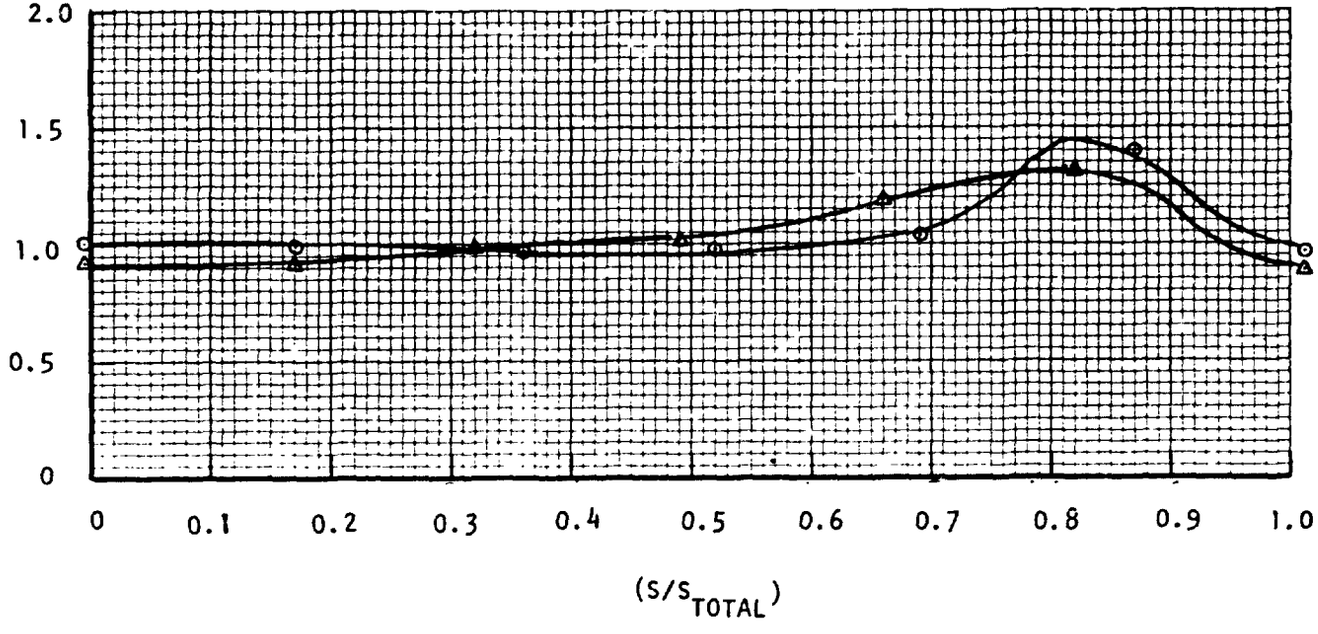

FIGURE 22B - EFFECT OF WAVE HEIGHT ON PRESSURE DISTRIBUTION

$M_\infty = 10.3$

$R_{e_\infty}/cm = 0.033 \times 10^6$

○ ε = 0.61 cm

△ ε = 0.29 cm

$\phi = 90°$

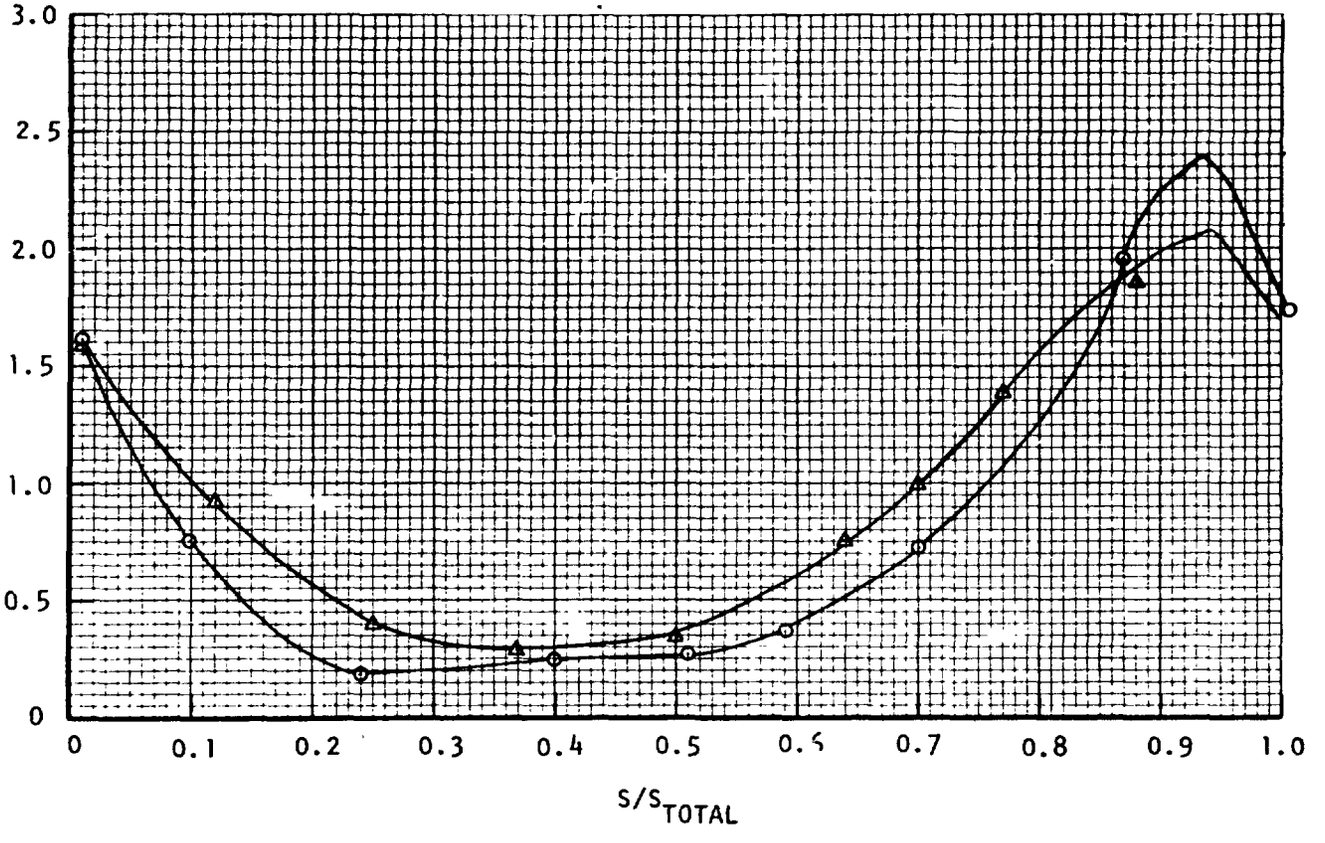

FIGURE 23A - EFFECT OF WAVE HEIGHT ON HEATING DISTRIBUTION

$M_\infty = 10.3$

$Re_\infty/cm = 0.033 \times 10^6$

O $\varepsilon = 0.61$ cm

$\Delta\ \varepsilon = 0.29$ cm

$\phi = 90°$

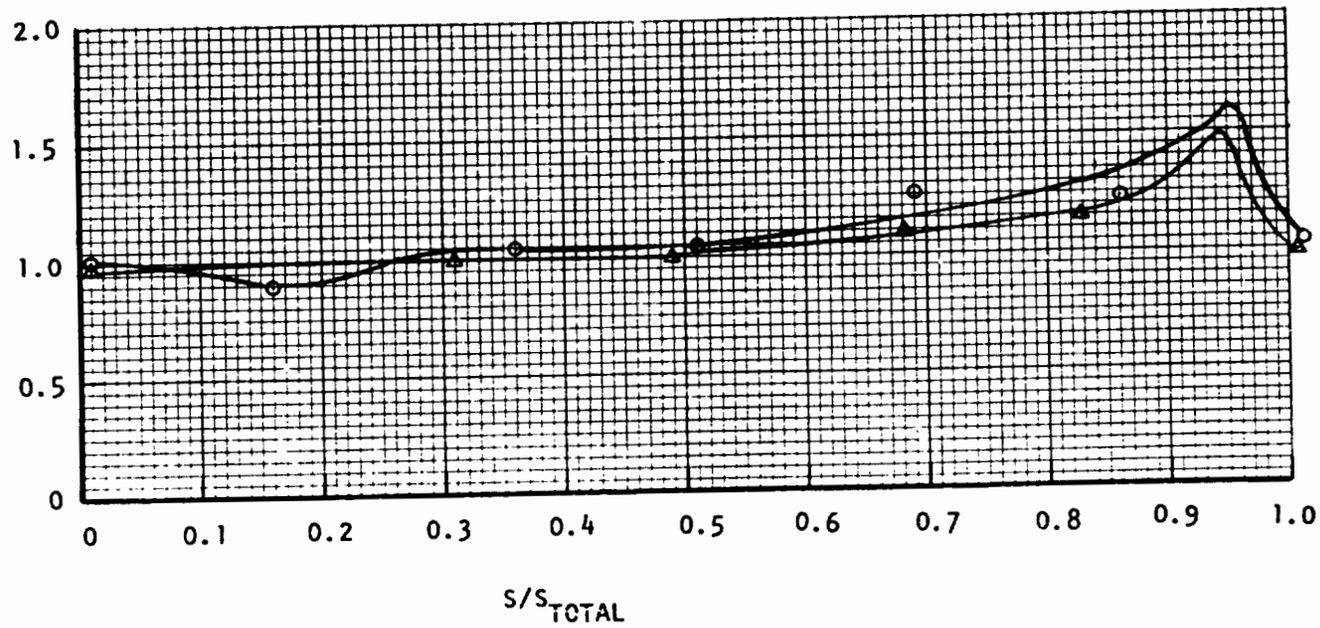

FIGURE 23B - EFFECT OF WAVE HEIGHT ON PRESSURE DISTRIBUTION

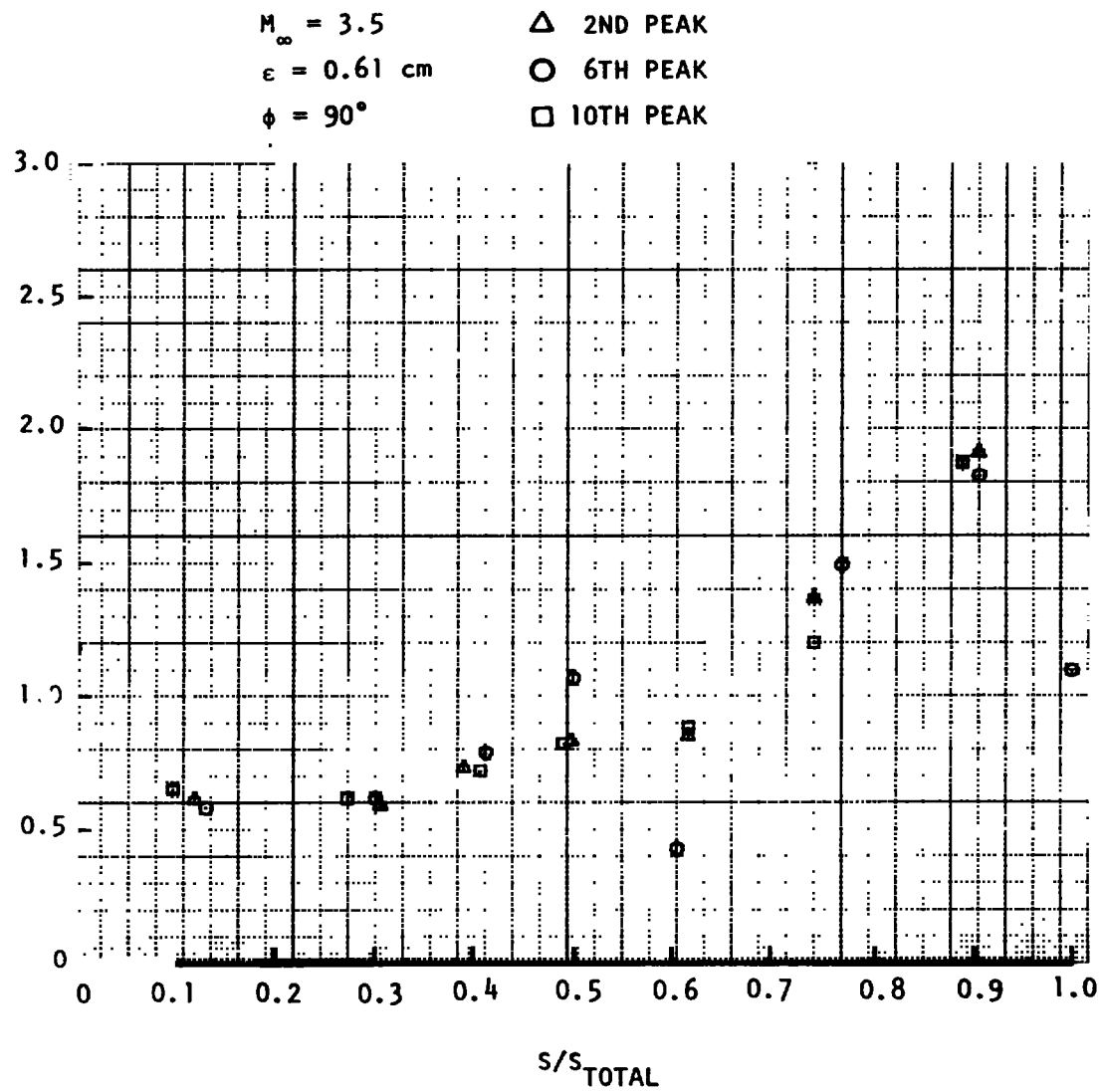

FIGURE 24A - EFFECT OF WAVE CYCLE ON HEATING DISTRIBUTION

$M_\infty = 3.5$

$\varepsilon = 0.61$ cm

O 2ND PEAK

Δ 10TH PEAK

$\phi = 90°$

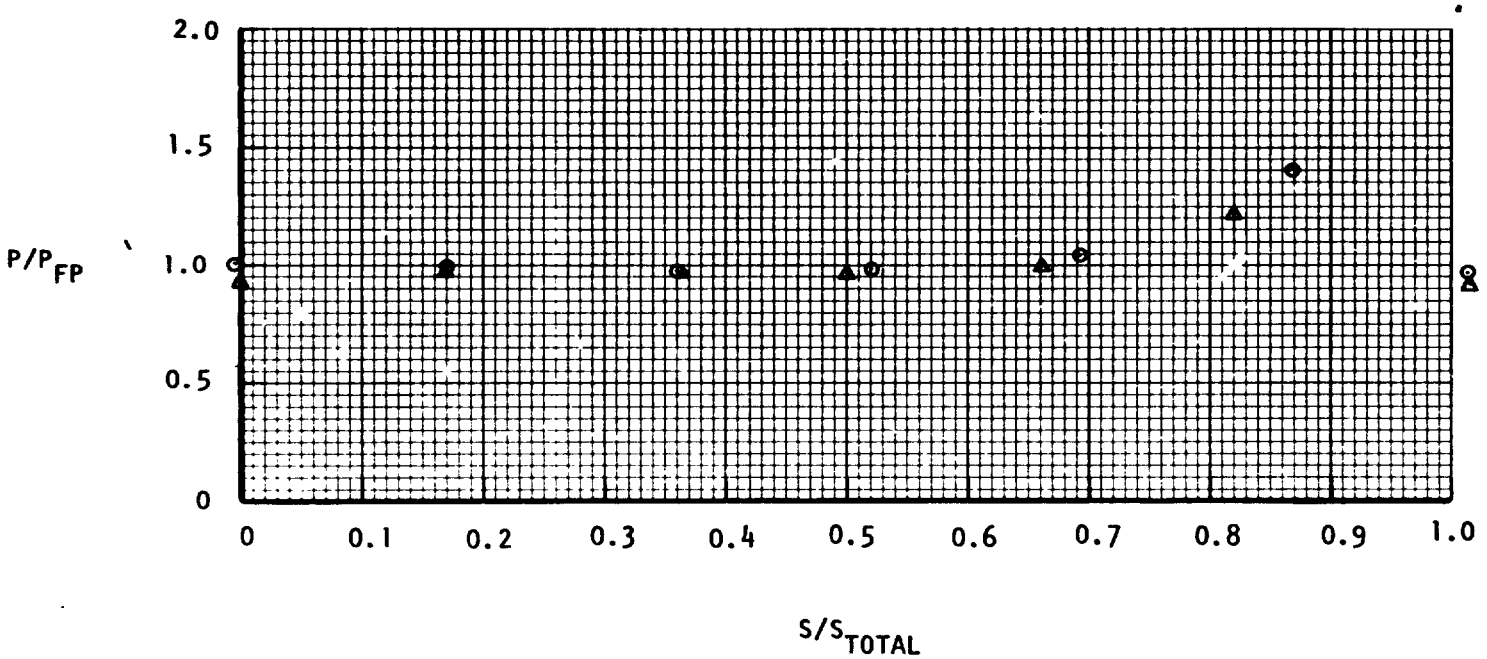

FIGURE 24B - EFFECT OF WAVE CYCLE ON PRESSURE DISTRIBUTION

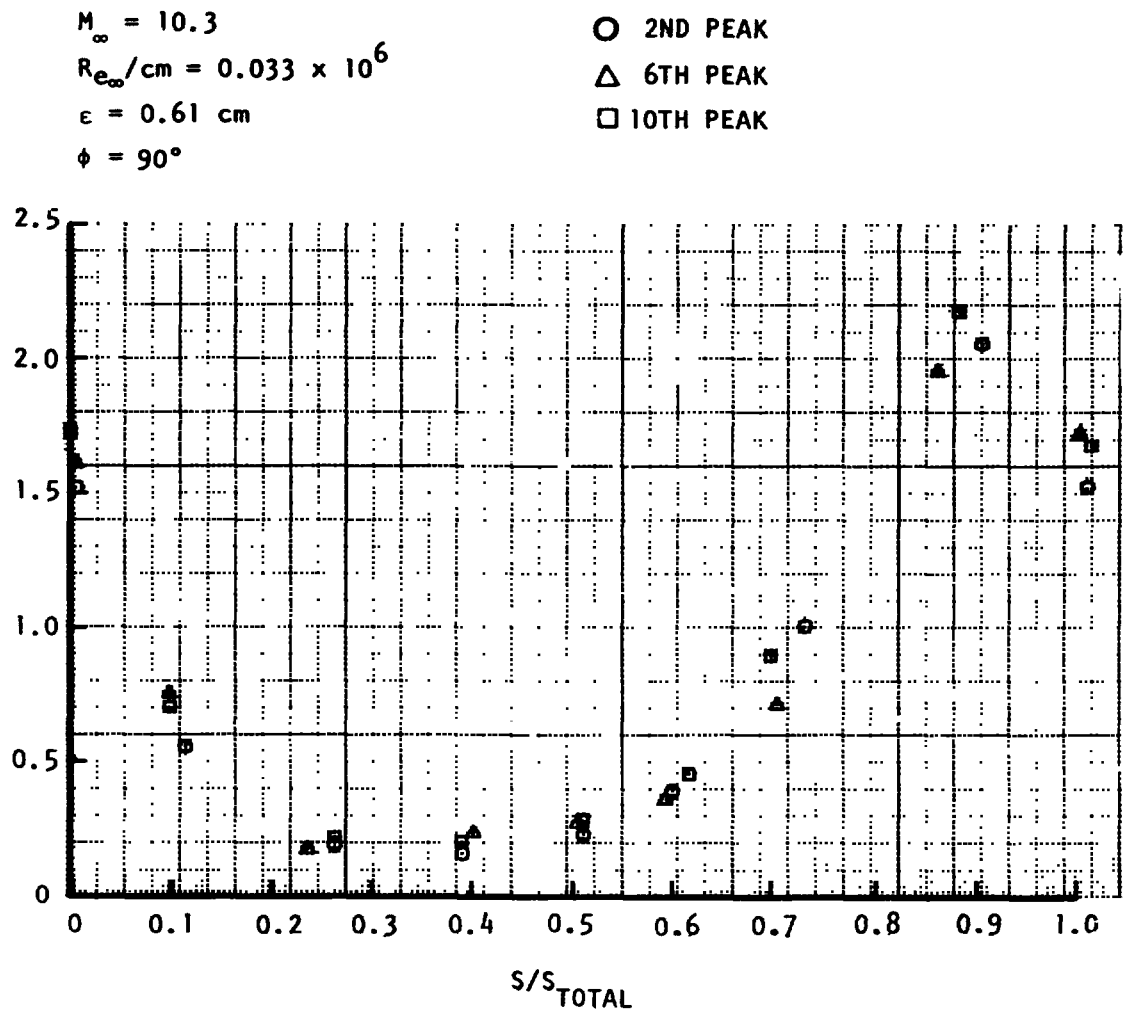

FIGURE 25A - EFFECT OF WAVE CYCLE ON HEATING DISTRIBUTION

$M_\infty = 10.3$

$R_{e_\infty}/cm = 0.033 \times 10^6$

$\varepsilon = 0.61$ cm

△ 2ND PEAK

O 10TH PEAK

$\phi = 90°$

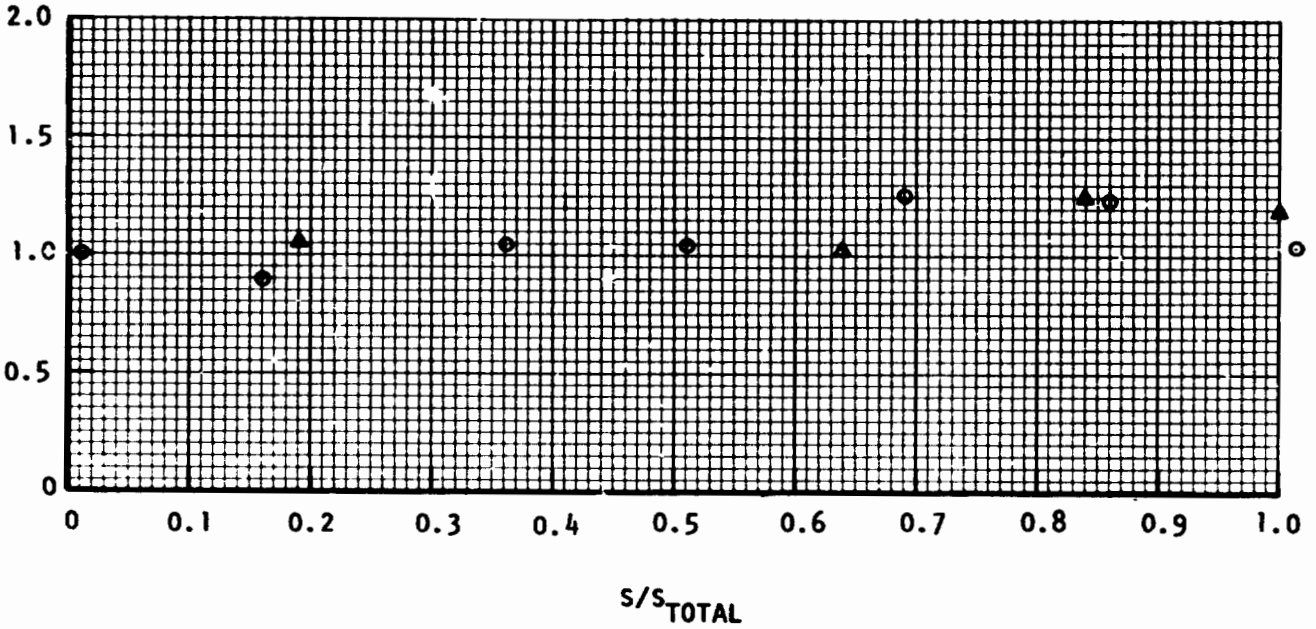

FIGURE 25B - EFFECT OF WAVE CYCLE ON PRESSURE DISTRIBUTION

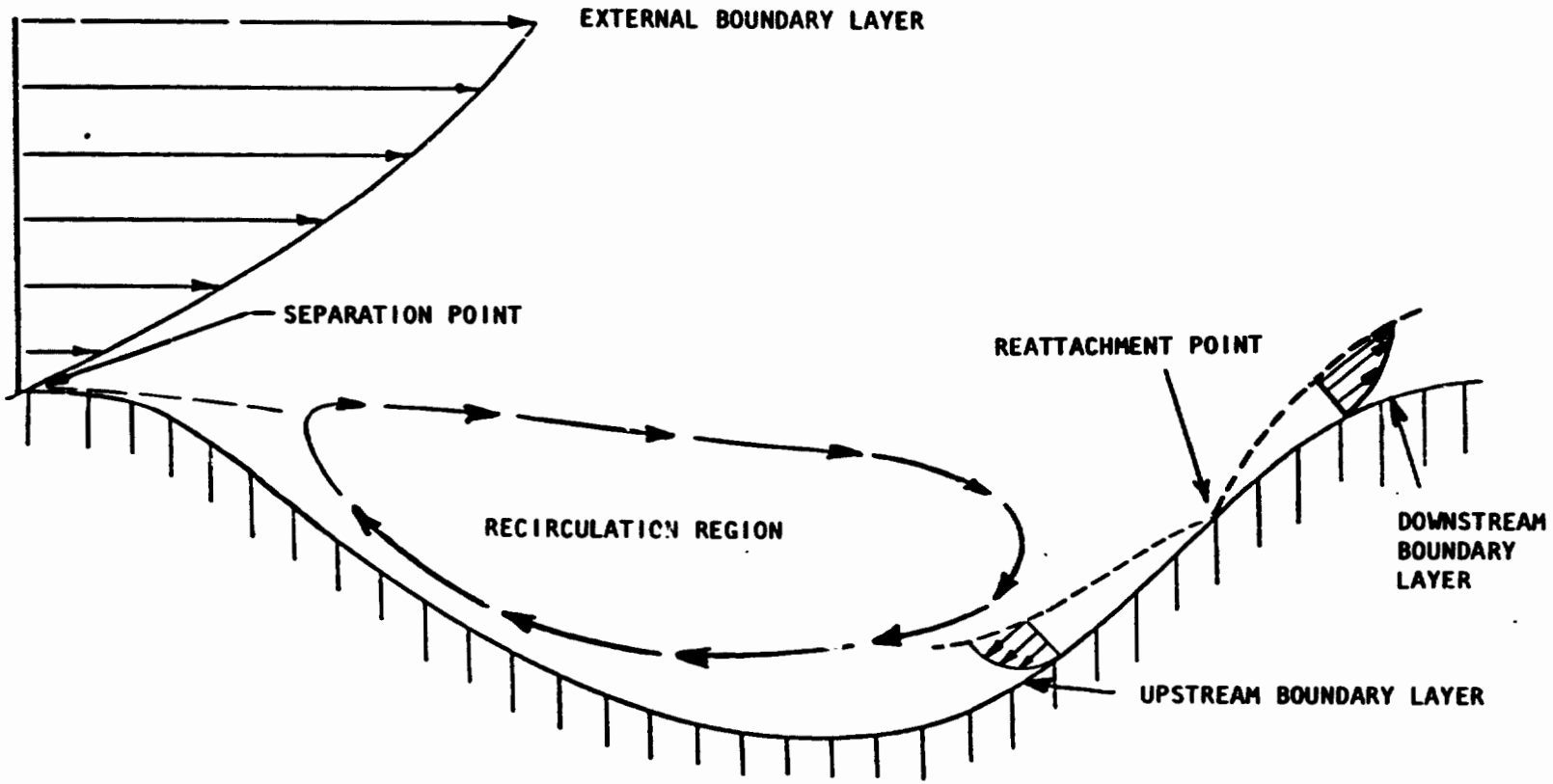

FIGURE 26 - FLOW MODEL

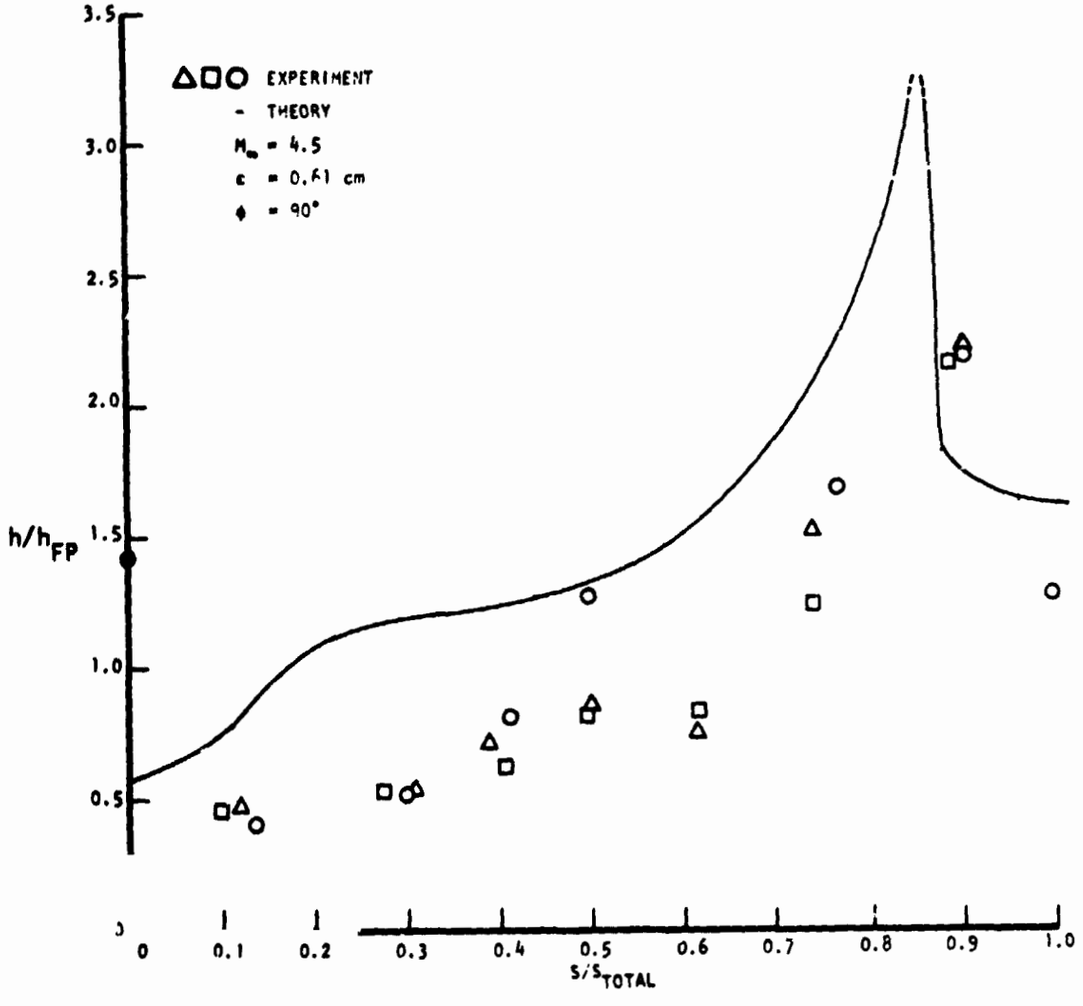

FIGURE 27 - COMPARISON OF EXPERIMENTAL AND THEORETICAL HEATING DISTRIBUTION

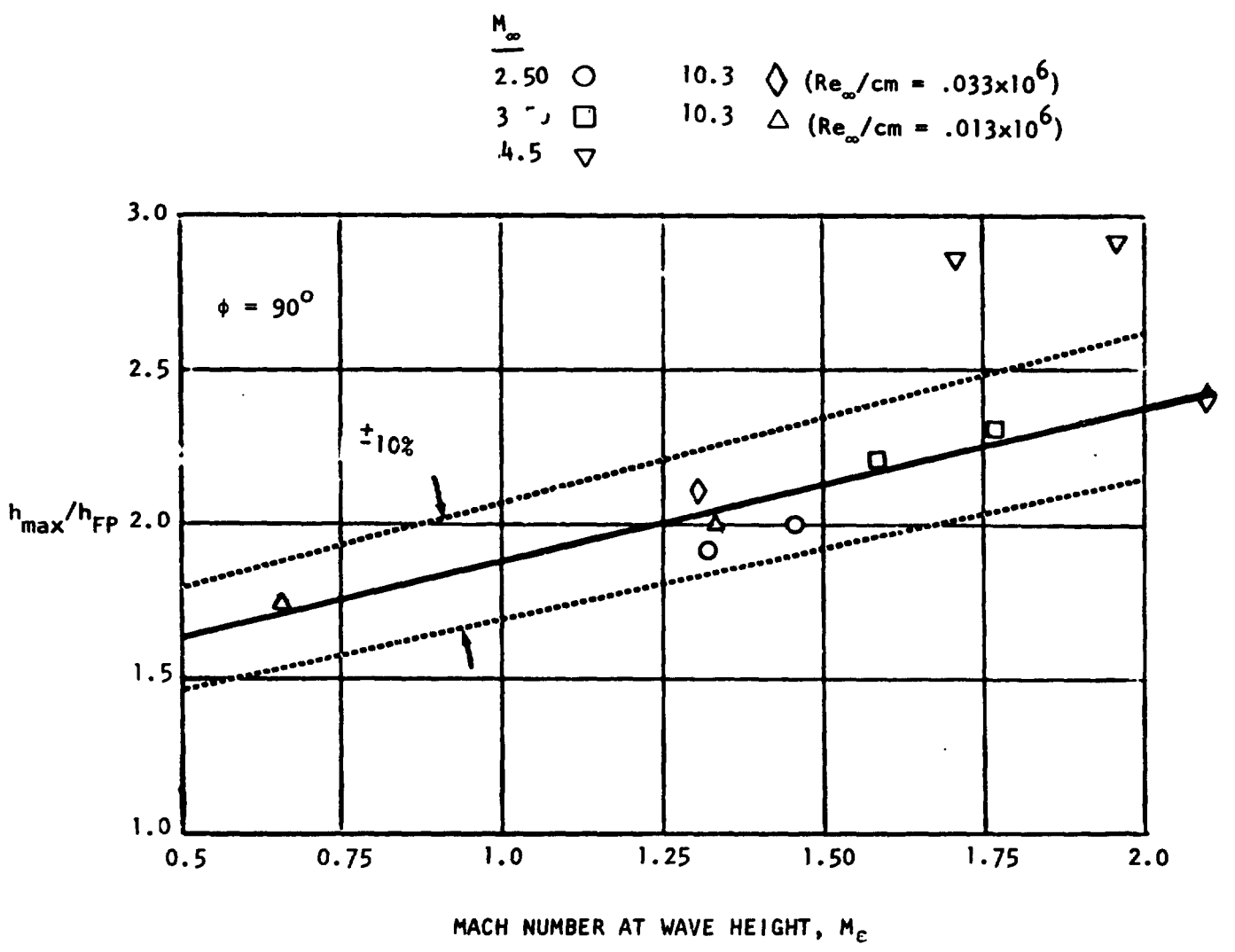

FIGURE 28 - CORRELATION OF PEAK HEATING IN TERMS OF MACH NUMBER AT WAVE HEIGHT

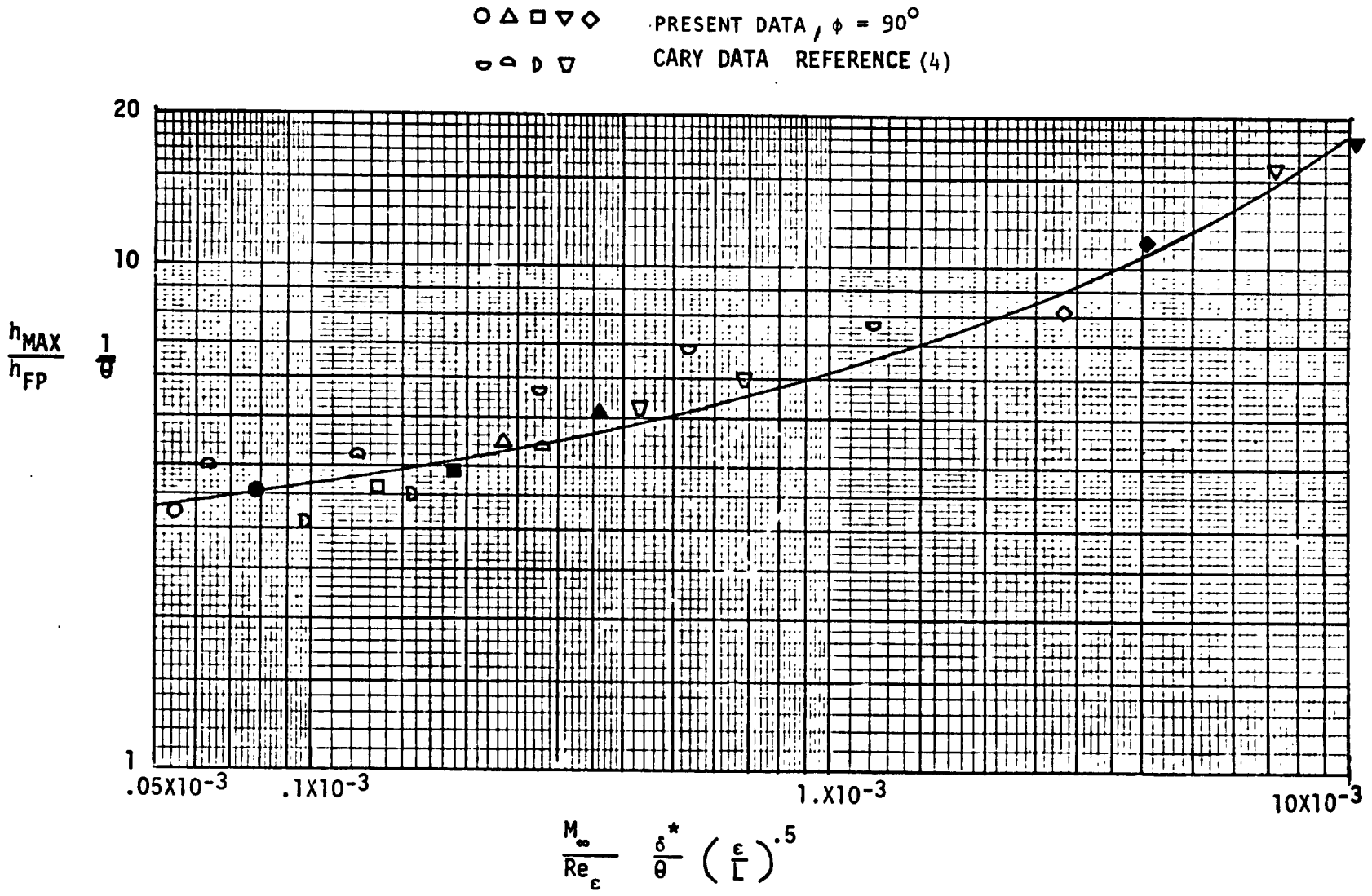

FIGURE 29 - CORRELATION OF MAXIMUM HEATING

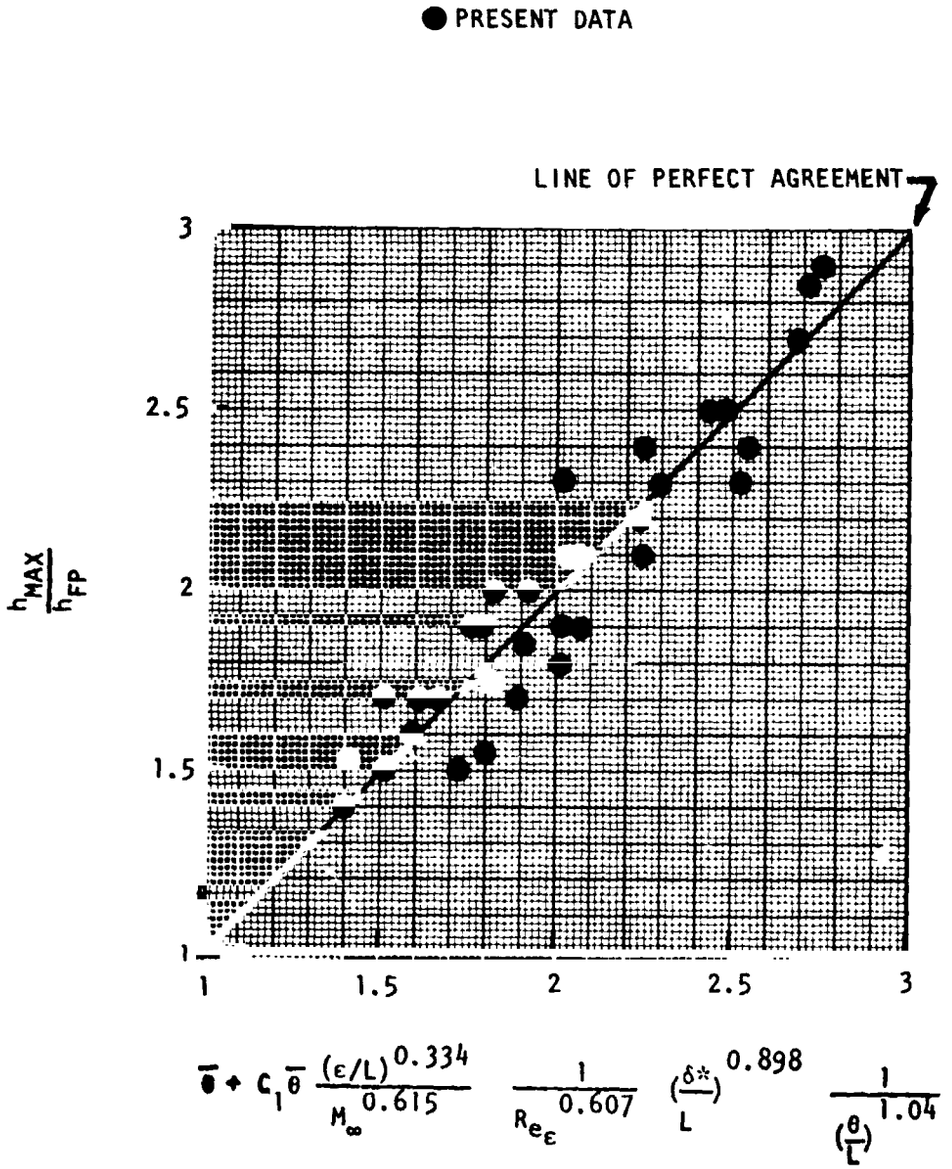

FIGURE 30 - CORRELATION OF MAXIMUM HEATING

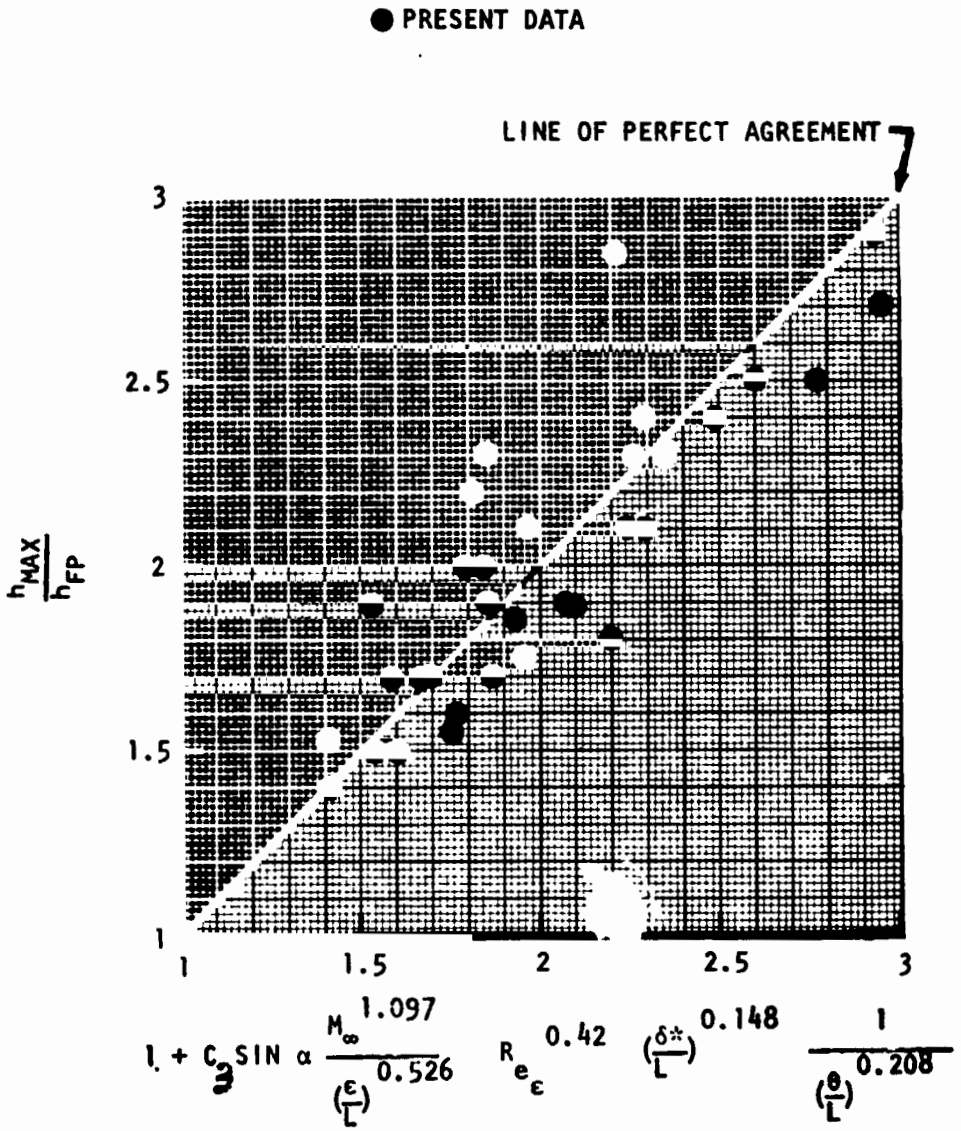

FIGURE 31 - CORRELATION OF MAXIMUM HEATING

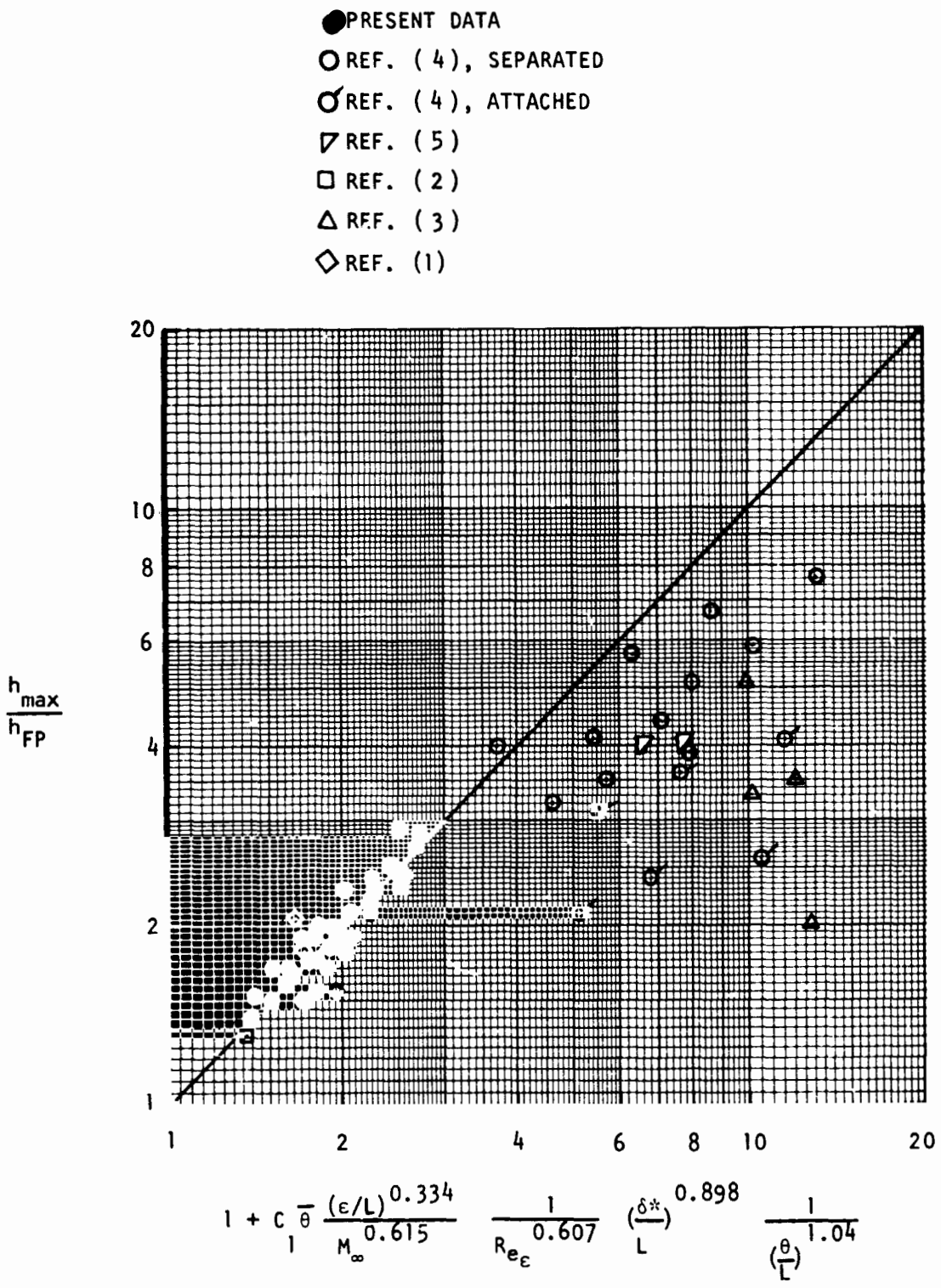

FIGURE 32 - CORRELATION OF MAXIMUM HEATING

● PRESENT DATA
○ REF. (4), SEPARATED
⊘ REF. (4), ATTACHED
▽ REF. (5)
□ REF. (2)
△ REF. (3)
◇ REF. (1)

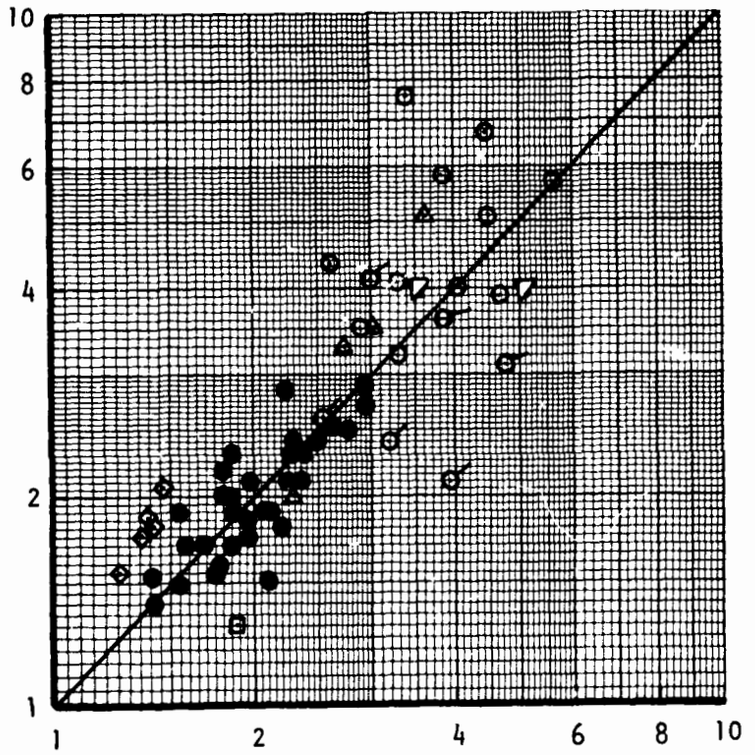

$\frac{h_{max}}{h_{FP}}$

$$1 + C_3 \sin\alpha \frac{M_\infty^{1.097}}{\left(\frac{\varepsilon}{L}\right)^{0.526}} R_{e_\varepsilon}^{0.42} \left(\frac{\delta^*}{L}\right)^{0.148} \frac{1}{\left(\frac{\theta}{L}\right)^{0.208}}$$

FIGURE 33 - CORRELATION OF MAXIMUM HEATING

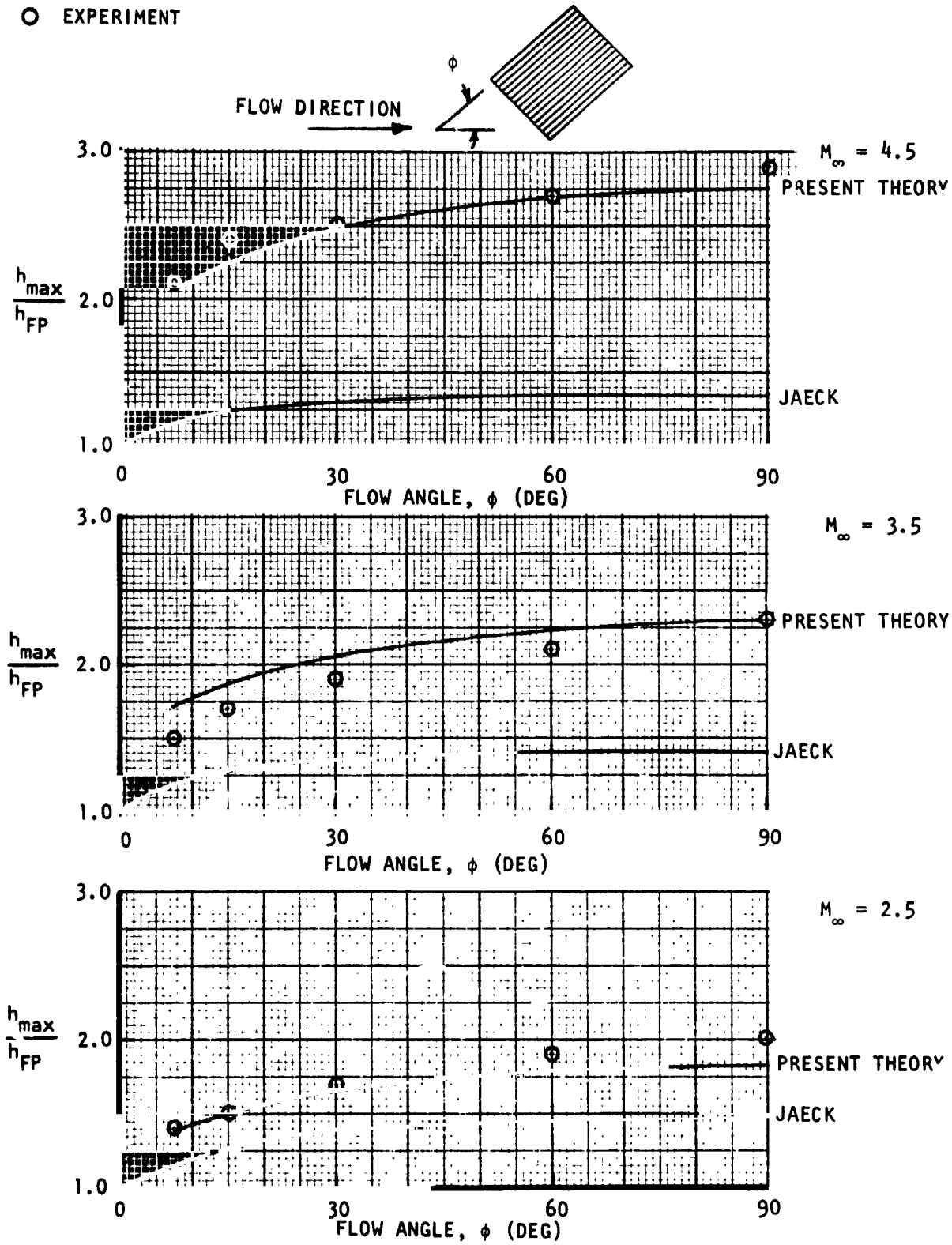

FIGURE 34 - MAXIMUM HEATING AS A FUNCTION OF THE FLOW ANGLE

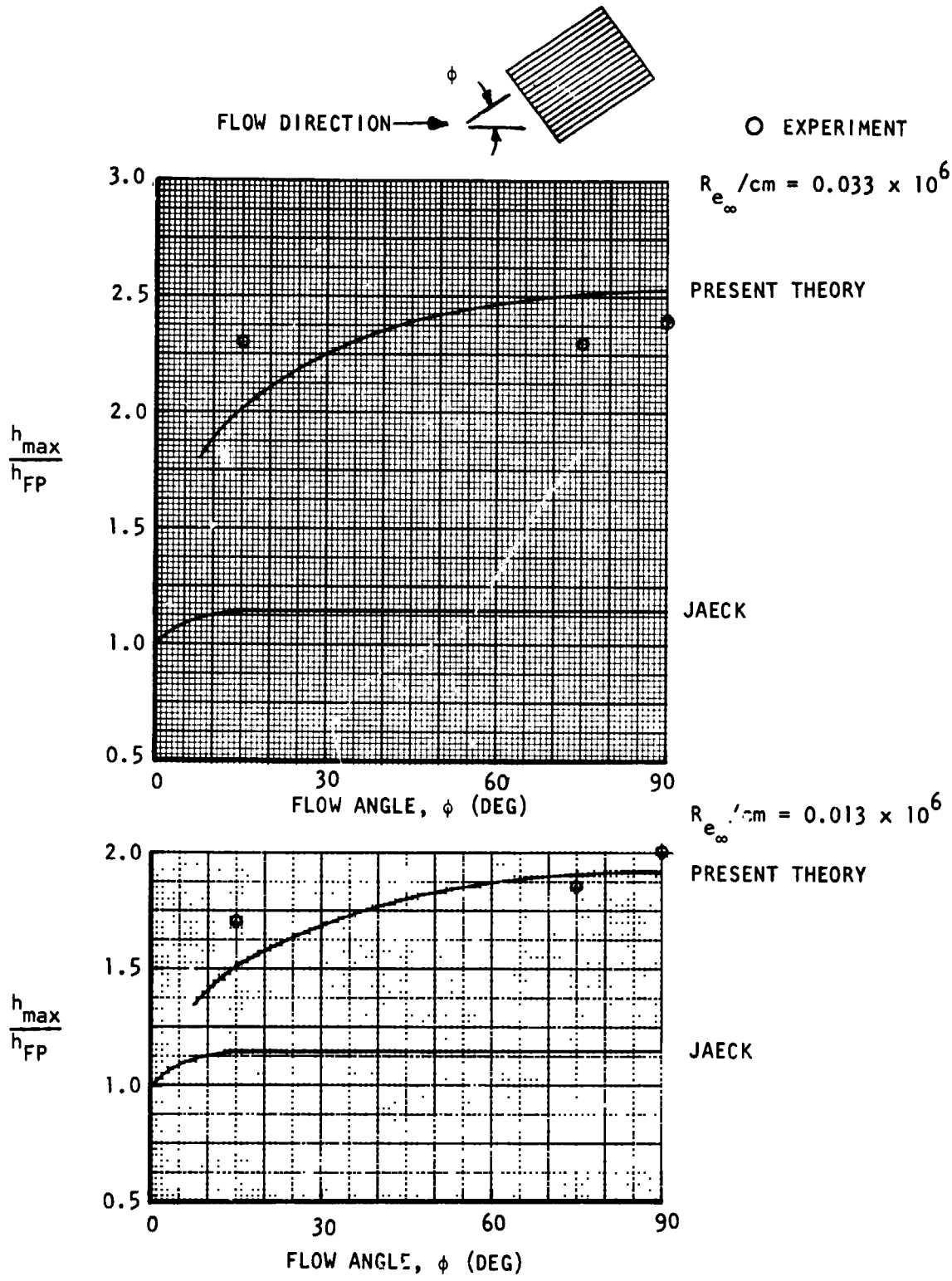

FIGURE 35 - MAXIMUM HEATING AS A FUNCTION OF THE FLOW ANGLE, M_∞ = 10.3

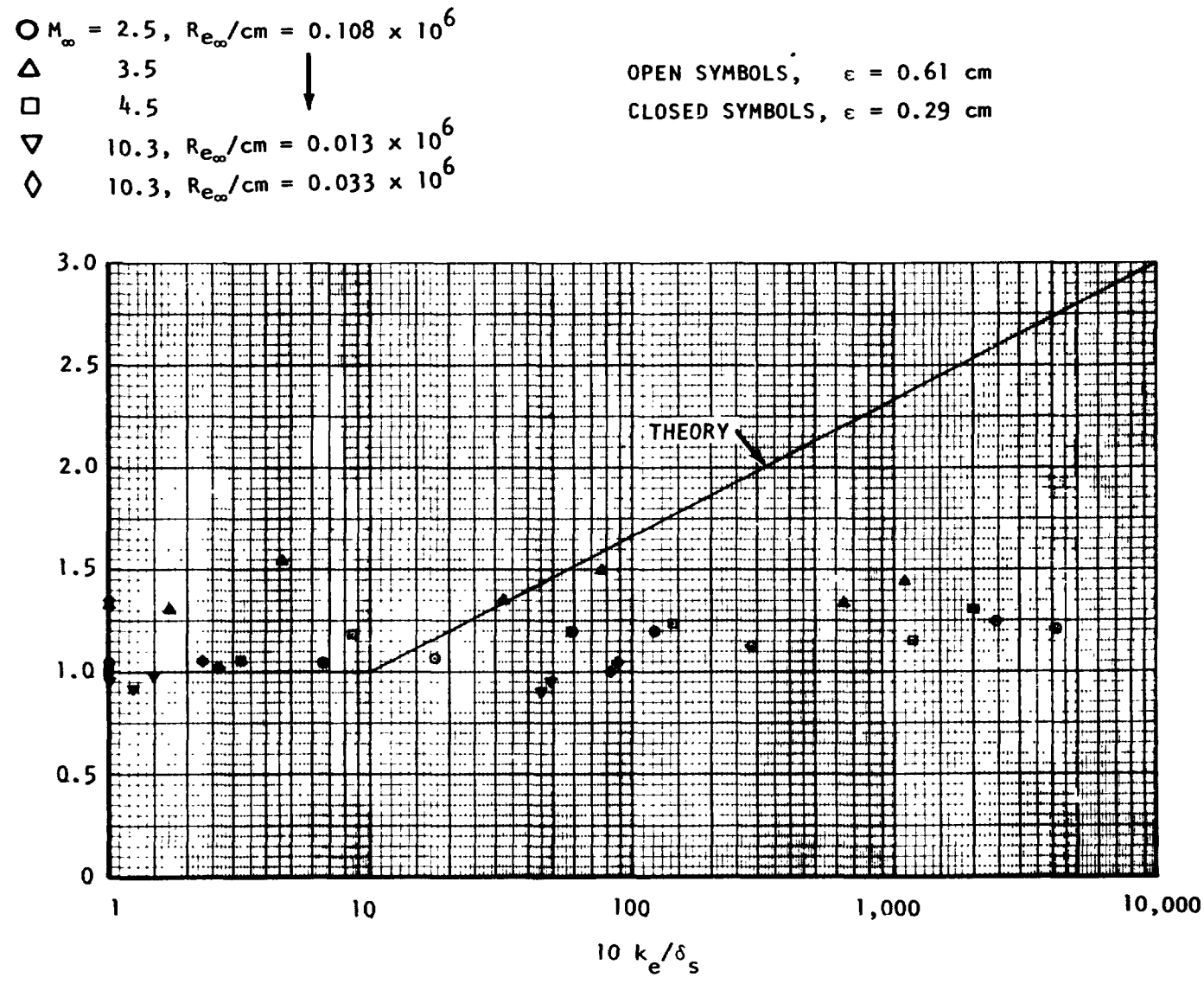

FIGURE 36 - AVERAGE HEATING COMPARED WITH POWARS CORRELATION

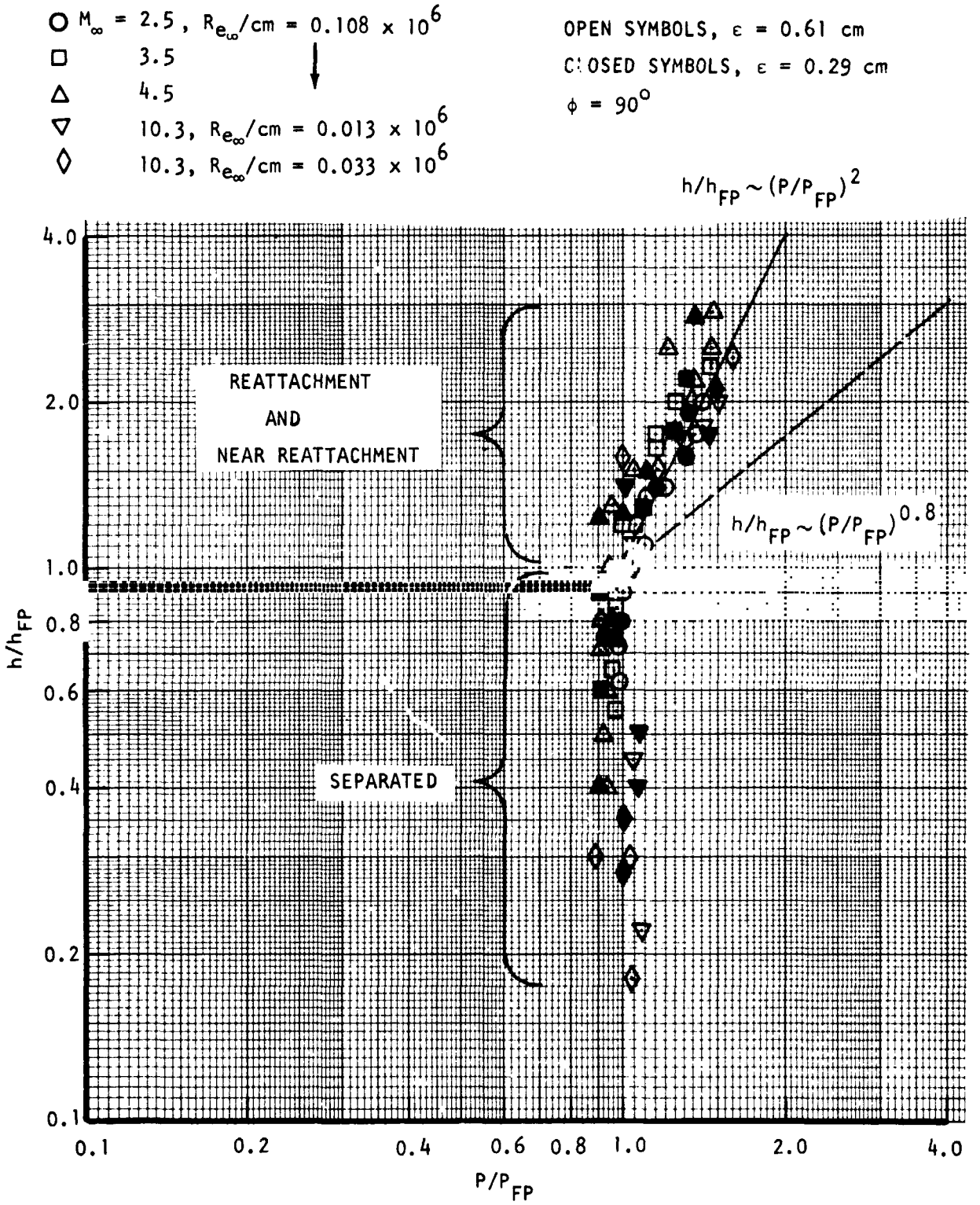

FIGURE 37 - CORRELATION OF HEATING AND PRESSURE DATA

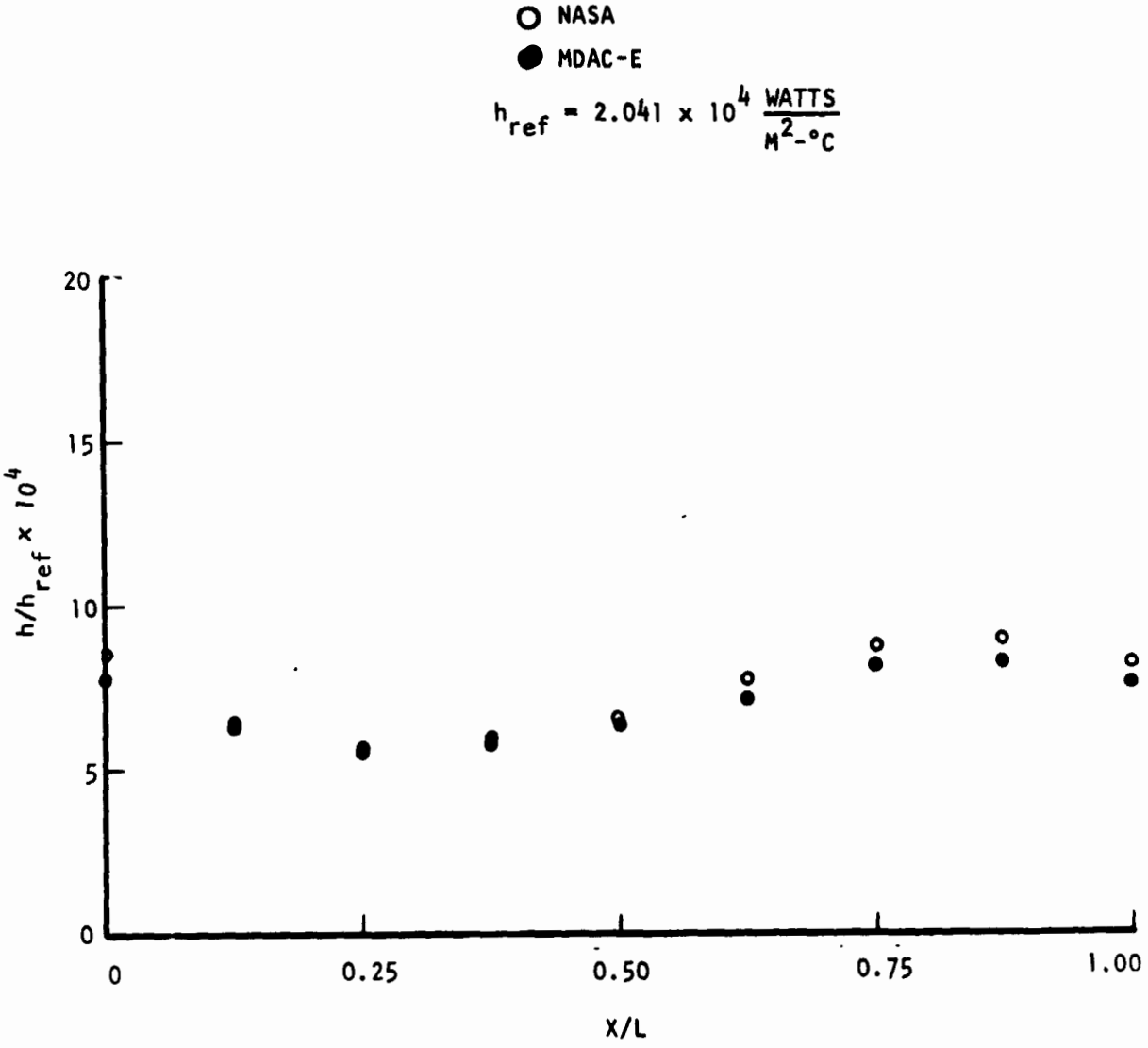

FIGURE A-1 - COMPARISON OF HEAT TRANSFER CALCULATIONS,

$\varepsilon = 0.61$ cm, $M_\infty = 4.5$, $\phi = 90°$

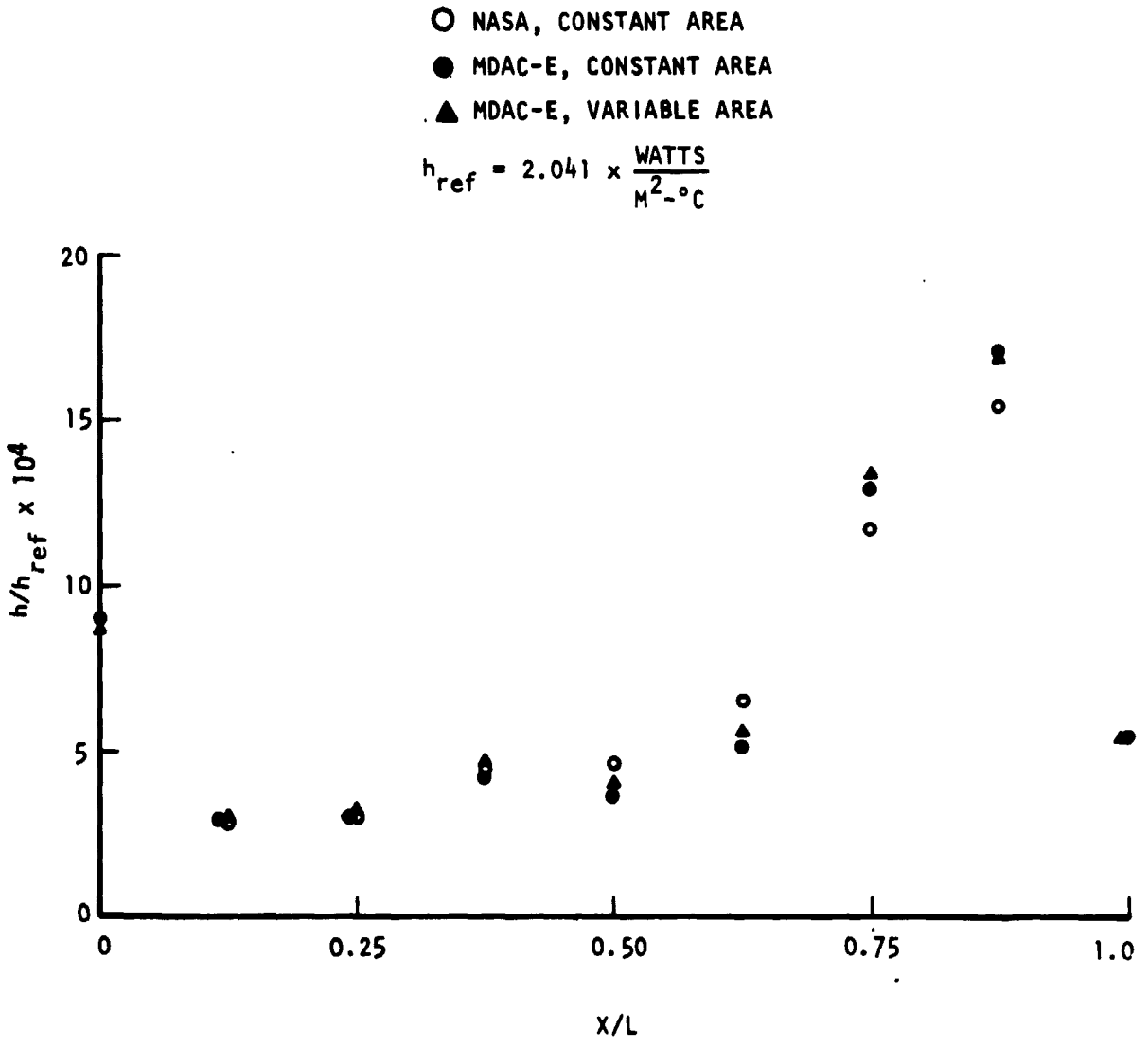

FIGURE A-2 - EFFECT OF VARIABLE AREA ON HEAT CONDUCTION CORRECTION,

$\varepsilon = 0.61$ cm, $M_\infty = 4.5$, $\phi = 90°$